Received October 23, 2020; accepted November 15, 2020. Date of publication 20 November 2020; date of current version 15 December 2020.

Digital Object Identifier 10.1109/OJCOMS.2020.3039536

Outage Performance of Pairwise NOMA Allowing a Dynamic Decoding Order and Optimal Pairs of Power Levels

VAN-LAN DAO (Graduate Student Member, IEEE), LE-NAM HOANG (Member, IEEE), SVETLANA GIRS (Member, IEEE), AND ELISABETH UHLEMANN (Senior Member, IEEE)

School of Innovation, Design and Engineering, Malardalen University, 722 14 Västerås, Sweden

CORRESPONDING AUTHOR: V.-L. DAO (e-mail: van.lan.dao@mdh.se)

This work was supported in part by the European Union's Horizon 2020 Research and Innovation Programme under the Marie Skłodowska-Curie Grant under Agreement 764785, FORA—Fog Computing for Robotics and Industrial Automation, and in part by the Swedish Foundation for Strategic Research (SSF) via the Project Future Factories in the Cloud (FiC).

ABSTRACT In this article, we evaluate the overall outage probability (OOP) of pairwise Non-orthogonal Multiple Access (NOMA) for both uplink and downlink. We also propose a dynamic decoding order (DDO) together with a fixed pairwise power allocation (FPPA) scheme, in which the optimal decoding order is decided based on the instantaneous channel gains, and thereafter, a pair of power levels is assigned in accordance with the selected decoding order. Exact closed-form expressions of the OOPs for both uplink and downlink pairwise NOMA considering all proposed decoding orders over Nakagami-m fading are derived. Further, we find the optimal fixed power levels for different power allocation strategies so that the OOPs are minimized. Moreover, we investigate the influence of the distances between the source nodes and the access point (AP), the target transfer rates and the path-loss exponents on the OOPs for all cases of decoding orders. In addition, we benchmark our proposed DDO against other decoding orders in terms of the OOP. The results show that assigning optimal fixed power levels which takes the instantaneous decoding order into account not only improves the communication reliability, but also reduces the complexity and computational load at the AP.

INDEX TERMS Overall outage probability, pairwise NOMA, dynamic decoding order, optimal power allocation, uplink/downlink NOMA.

I. INTRODUCTION

RECENTLY, beyond 5G/6G techniques have attracted much attention, in which some technologies, e.g., Non-Orthogonal Multiple Access (NOMA), massive multiple-input-multiple-output and reconfigurable intelligent surface have become potential key technologies [1]–[3], and the combination of one or more of these techniques can bring additional benefits [4], [5]. Moreover, emerging industrial applications have a need for ultra-low latency, high reliability and often also energy efficiency. Due to this, delays caused by waiting for channel access, or reliability problems due to collisions when several nodes are attempting to access the channel at the same time, severely affect the performance. Consequently, there is a drive to design more spectrally and energy efficient multiple access schemes, which enable channel access with high reliability and low delay for use in future wireless networks.

The fundamental concept of NOMA is to remove the orthogonality in between the different users so that multiple users can be served simultaneously by sharing the same, often limited, system resources. The superior spectral efficiency of NOMA which helps reduce the latency of communication is shown in [6]. With NOMA, an access point (AP) can communicate in both downlink and uplink transmission phases with many users at the same time using the same frequency, and instead separating the users in a different domain. In this article, we consider NOMA in the power-domain, implying that the users are separated using different transmit power levels.

To decode signals from many users that are using the same frequency at the same time, the key idea of NOMA in the power-domain is to multiplex the transmitted signals at different power levels in such a way that successive interference cancellation (SIC) unit(s) [7] can be employed at the receiver(s). While the SIC unit is included at the AP to decompose uplink signals, for downlink NOMA the users are supposed to perform SIC. However, the SIC process is a complex operation and becomes even more complicated with increased number of users. Therefore, to reduce the complexity as well as cost of the receivers, the number of active NOMA users at the same time should not be too large [8]. Due to this practical constraint, many previous papers have evaluated the performance of pairwise NOMA, i.e., NOMA with at each time-frequency instance only two users transmitting to an AP in the uplink phase, or receiving a superimposed signal from the AP in the downlink phase [9]–[14]. In this scenario, efficient user pairing plays an important role [15] and thus proper selection of the users for pairing has attracted much attention in the literature [16]. Pairwise NOMA is also useful for enhancing the system performance in industrial systems, where it can be used in combination with an existing multiple access technology like Time Division Multiple Access (TDMA) to increase the number of nodes that can get access to the channel at each time instance [13]. Given a good selection of the pairs, pairwise NOMA in the power-domain is therefore a solution of high practical importance for future systems, which is why we focus on it in our work.

With NOMA in the power-domain, the power allocation strategy inevitably plays an important role and significantly affects the system performance [17]. There are two types of power allocation strategies: fixed power allocation (FPA) and dynamic power allocation (DPA) [17]–[19]. With FPA, each user is allocated the same power level for every transmission. On the other hand, the power level for each user can be adjusted based on its instantaneous channel state information (CSI) [18] when using a DPA strategy. To optimize performance, a flexible decoding order, i.e., which signal that should be decoded first and subsequently removed from the superimposed signal, is also important. In other words, a receiver must know and follow an intended decoding order [20]. This is also the case for pairwise NOMA. In the literature, several types of decoding orders have been proposed, e.g., random [21], fixed [22], [23] and dynamic decoding order [24]–[26], while the criteria used for ordering are the distances [22], [23], the received powers [25]–[27] or the quality of service (QoS) [28], [29].

To evaluate the performance of NOMA, the outage performance in terms of individual outage probability (IOP) and overall outage probability (OOP) is often used. For industrial applications, where each sensor-controller or controller-actuator link matters, it is often important to evaluate the IOP. The benefit of the OOP however, is that we get one measure for the entire network, which is good for evaluating the performance of larger sensor networks, but also for industrial settings when selecting system parameters such as a suitable power allocation to the different nodes, ensuring short-term user fairness, which is of essence for real-time constraints. Hence, much attention has been given to derive closed form expressions for the IOP and OOP. However, a comprehensive comparison in terms of the OOP considering all different types of decoding orders and power allocation strategies has not yet been studied for both uplink and downlink NOMA.

A. RELATED WORKS

Closed-form expressions for the OOP for downlink NOMA was first introduced in [30], [31] under the assumption that the users can be ordered based on the channel gains. However, as the channel gains vary from time to time, the calculations of the OOP in these papers are accurate only when the variation of the channel gain at each user is small enough to not affect the decoding order. This assumption becomes asymptotically reasonable when the pair consists of one cell-center node and one cell-edge node. This type of decoding order selected based on the distances between the AP and users is further elaborated on in the calculations in [22], [23]. We term this decoding order fixed decoding order (FDO), implying that the long term statistic of the CSI, or the fixed distances between the AP and users, is used as the criterion for determining the order of decoding. Another FDO based on the QoS requirements of the users such as their targeted data rates is introduced in [28], [29]. In contrast, a scheme with a dynamic decoding order (DDO) is proposed in [24], [27] but using FPA, i.e., the same power level is assigned for each user every time. Moreover, the authors in [24] also investigate the OOP for a DDO-DPA scheme in downlink pairwise NOMA and show that it is better than a DDO-FPA scheme. However, since the pair of fixed power levels used for the DDO-FPA scheme when comparing to the DDO-DPA scheme in [24] is far-inferior to the optimal pair, it cannot show the whole benefit of using the DDO-FPA scheme.

For uplink NOMA, a scheme using a DDO based on the instantaneous received powers is proposed in [25]–[27]. In particular, [25], [26] prove that in terms of the IOP, the scheme using a DDO is better than the FDO scheme. Here, the considered FDO scheme uses the long term statistics of the channel gains as the criterion for ordering. The authors in [27] further calculate the OOP for uplink NOMA over Nakagami-m fading channels using the same DDO scheme as proposed in [25], [26]. However, it should be noted that the power allocation strategy in [25]–[27] is fixed, such that the source node experiencing higher path-loss always gets lower power compared to the other source node, and thus no previous work has examined the OOP for a DDO-DPA scheme in the uplink.

B. MOTIVATIONS AND CONTRIBUTIONS

As seen from the related works, a comprehensive and fair comparison between different NOMA schemes considering

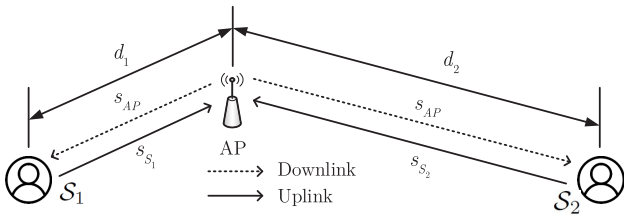

FIGURE 1. System model.

TABLE 1. Notation summary.

Notation	Description
d_i	Distance between the two source nodes and the AP, $i \in \{1, 2\}$
g_i	Nakagami-m fading channel coefficient of the ($\mathcal{S}_i \longrightarrow$ AP), (AP $\longrightarrow \mathcal{S}_i$) communication link
n_j	Additive white Gaussian noise at $\mathcal{S}_1$, $\mathcal{S}_2$, and AP, respectively, $j \in \{\mathcal{S}_1, \mathcal{S}_2, AP\}$, modeled as $n_j \sim CN(0, \sigma_0^2)$
P_{dl}	The total power that AP transmits to the two users in downlink pairwise NOMA, $P_{dl} = P_1^d + P_2^d = \text{const}$
P_{ul}	Total transmit power of the two source nodes $\mathcal{S}_1$ and $\mathcal{S}_2$ in uplink paiwise NOMA, $P_{ul} = P_1^u + P_2^u = \text{const}$
ζ_i	Path-loss exponent

the effects of both decoding orders and power allocation strategies has not yet been studied. In addition, the complexity constraint should be taken into account when determining the optimal settings based on the instantaneous channel conditions. It is clear that the DDO-DPA scheme performs best in terms of the OOP, but it has a very high complexity. The DDO-FPA scheme has lower complexity compared to the DDO-DPA scheme but still performs better in terms of OOP than all the FDO schemes. However, given that the decoding order in pairwise NOMA only changes between two different states, it motivates using two different but fixed pairs of power levels adjusted to each of the two corresponding decoding orders. This scheme was partly investigated in [27] for downlink NOMA, but the DDO-DPA scheme becomes impractical for the uplink, even for pairwise NOMA. The reason is that before each transmission, the AP is supposed to inform each source node about its power allocation action. This can lead to higher latency, larger communication cost, and abundant overhead with more complex protocols. To this end, our major contributions are summarized as follows:

- We propose a DDO strategy with two simple steps before each transmission: first the optimal decoding order is decided at the AP based on the instantaneous channel gains, and second, the power allocation scheme is selected from a fixed predetermined set in accordance with the chosen decoding order. The proposed scheme is termed DDO-fixed pairwise power allocation (FPPA) given that only two pairs of fixed power levels are used interchangeably. This implies that the complexity is reduced and also that the communication costs are reduced to selecting one pair from a set of two pairs.
- Closed-form expressions of the OOP for all types of decoding orders and all power allocations are derived for both uplink and downlink pairwise NOMA over the Nakagami-m channel. In contrast to [24], the calculations use a proposed general theorem and the Venn diagram method to consider all possible cases, taking into account the target data rates of the users, their path-loss exponents, the distances between the AP and the nodes, as well as the power allocation strategies. We use the OOP to benchmark our DDO-FPPA scheme against the state-of-the-art approaches for selecting the decoding order and the power allocation for pairwise NOMA.
- We propose algorithms which can find the optimal power allocation for each user in both uplink and downlink pairwise NOMA, given a certain decoding order to be used for the fixed set. We found that assigning more power to the weaker user not only gains performance in terms of communication reliability, but also reduces complexity and computational load at the AP. We also consider the complexity of finding the optimal values and whether or not the extra complexity is worth it.
- Finally, using the derived closed-form expressions and the proposed algorithms, we investigate the effects of several different parameters, i.e., path-loss exponents, user distance, power allocation strategy, and target data rates on the OOP with and without the optimal power levels.

The rest of this article is organized as follows. The system model is described in Section II, followed by the proposed decoding orders combined with power allocation strategies in Section III. Then, Section IV presents the calculation of the OOP for both uplink and downlink pairwise NOMA and thereafter the optimal power allocation problems are solved in Section V. Next, numerical results are presented in Section VI. Finally, Section VII concludes this article.

II. SYSTEM MODEL

In this article, we consider a system consisting of two nodes $\mathcal{S}_i$, $i \in \{1, 2\}$ and one AP as shown in Fig. 1. The descriptions of the notations used in Fig. 1 are provided in Table 1. The channels are assumed to be Nakagami-m fading, which can describe a wide number of fading contexts such as Rayleigh, Rician by adjusting its parameters. Therefore, the channel gains $|g_i|^2$ can also be characterized by a Gamma distribution with shape m_i and unit mean. Without loss of generality, we assume $d_1 \leq d_2$. Moreover, we consider that all nodes operate in half-duplex mode with a single antenna, a reasonable assumption in industrial settings. Another assumption used in our work is that the CSIs are perfectly known at the AP. In the uplink phase, both source nodes transmit their messages to the AP using the same time-frequency resource but different power levels. The received signal at the AP is given as

$$y_{AP} = \sqrt{P_1^u} g_1 s_{\mathcal{S}_1}^u + \sqrt{P_2^u} g_2 s_{\mathcal{S}_2}^u + n_{AP}, \tag{1}$$

where P_1^u, P_2^u, and $s_{\mathcal{S}_i}^u$ are the transmit power of $\mathcal{S}_1$, $\mathcal{S}_2$, and uplink signal of $\mathcal{S}_i$, respectively. Before all transmissions, the AP first decides on the decoding order based on the CSIs and then assigns a power level to each source node in accordance with this decoding order. Suppose that the AP decodes $s_{\mathcal{S}_i}^u$ first, it will consider $\sqrt{P_{i'}^u} g_{i'} s_{\mathcal{S}_{i'}}^u + n_{AP}$, $i' \neq i$ as noise. If $s_{\mathcal{S}_i}^u$ is decoded successfully, $\sqrt{P_i^u} g_i s_{\mathcal{S}_i}^u$ is subtracted from y_{AP} and $s_{\mathcal{S}_{i'}}^u$ can be decoded with n_{AP} as the only noise.

During the downlink phase, the AP broadcasts one superimposed signal s_{AP} of the two messages $s_{\mathcal{S}_i}^d$ intended for the two users:

$$s_{AP} = \sqrt{P_1^d} s_{\mathcal{S}_1}^d + \sqrt{P_2^d} s_{\mathcal{S}_2}^d, \tag{2}$$

where P_1^d and P_2^d are the power levels assigned to $\mathcal{S}_1$ and $\mathcal{S}_2$, respectively. The received signal at $\mathcal{S}_i$ is given as

$$y_{\mathcal{S}_i} = g_i s_{AP} + n_{\mathcal{S}_i}. \tag{3}$$

In downlink pairwise NOMA, the decoding order is also decided first and each receiver is allocated power based on this order. However, this decoding order is different from that of uplink NOMA. Here one of the receivers, $\mathcal{S}_i$, is selected to utilize SIC. At this receiver, the message of the other receiver, $\mathcal{S}_{i'}$, is decoded first, considering $\mathcal{S}_i$'s message as interference. When $s_{\mathcal{S}_{i'}}^d$ is successfully decoded, $\sqrt{P_{i'}^d} g_i s_{\mathcal{S}_{i'}}^d$ will be subtracted from $y_{\mathcal{S}_i}$ and $\mathcal{S}_i$ can decode its own message with $n_{\mathcal{S}_i}$ as the only noise. Meanwhile, at $\mathcal{S}_{i'}$, the other receiver not performing SIC, its designated message is decoded by considering $\sqrt{P_i^d} g_{i'} s_{\mathcal{S}_i}^d$ as interference.

III. DECODING ORDER AND POWER ALLOCATION

Most previous publications have considered an FDO based on d_i. Here we propose a DDO scheme based on the instantaneous normalized channel gains. Suppose that at one time-frequency instance, we have $d_i^{-\zeta_i}|g_i|^2 \geq d_{i'}^{-\zeta_{i'}}|g_{i'}|^2$, $i \neq i'$, then $\mathcal{S}_i$ will do SIC in the downlink, while in the uplink the AP will first decode $\mathcal{S}_i$'s signal considering $\mathcal{S}_{i'}$'s signal as noise. Given that $d_1 \leq d_2$, the probability that the FDO based on distance and the proposed DDO give the same result of ordering is as follows:

$$p_{RO} = \Pr\left\{d_1^{-\zeta_1}|g_1|^2 \geq d_2^{-\zeta_2}|g_2|^2\right\} = \Pr\{\rho_1 \geq \rho_2\}, \tag{4}$$

where $\rho_i = d_i^{-\zeta_i}|g_i|^2$ can be modeled as a Gamma distribution, $\rho_i \sim G(m_i, \frac{d_i^{-\zeta_i}}{m_i})$. In Fig. 2, we illustrate p_{RO} as a function of d_2 and ζ_i with $d_1 = 150$m and $m_1 = m_2 = 1$. It is clear that p_{RO} always reaches 1 when $d_2 \gg d_1$. Also, we can see that when $\mathcal{S}_1$ and $\mathcal{S}_2$ are in the same environment, i.e., $\zeta_1 = \zeta_2$, p_{RO} reaches 1 faster in an environment with higher ζ_i. Moreover, p_{RO} reaches 1 even faster when $\zeta_2 > \zeta_1$. However, when $\zeta_2 < \zeta_1$, p_{RO} is approximately 0 with $d_2 \approx d_1$ and slowly reaches 1 for a very high d_2. Hence, there exists a situation when $p_{RO} \ll 1$ that needs to be addressed. Moreover, the power allocation coefficient for each source node is an important factor that affects the system performance [20], [32], [33] as it can be used to compensate for the path-loss.

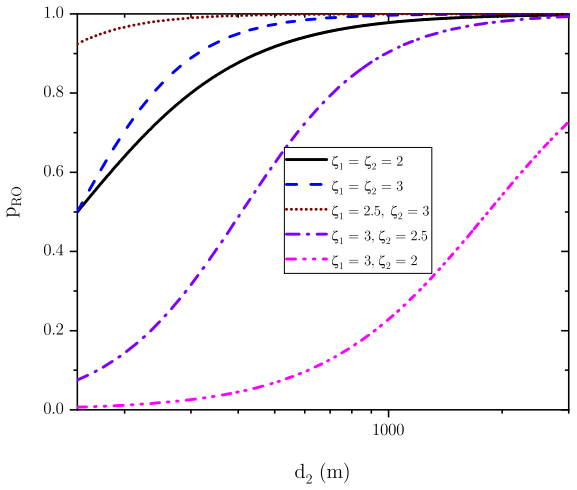

FIGURE 2. The probability p_{RO} that FDO and DDO gives the same result versus d_2.

A. DOWNLINK PAIRWISE NOMA

In this work, we propose the DDO-FPPA scheme in which the user with higher instantaneous normalized channel gain first decodes the other user's signal and then performs SIC to obtain its own signal without interference. Accordingly, the power assigned to the receiver performing SIC is always lower than at the other receiver. Once the AP knows $\frac{|g_1|^2}{d_1^{\zeta_1}}$ and $\frac{|g_2|^2}{d_2^{\zeta_2}}$, it can decide on the appropriate decoding order, and accordingly, the pair of power levels allocated to the two users. With DDO-FPPA, the rates obtained by $\mathcal{S}_1$ and $\mathcal{S}_2$ with $\frac{|g_1|^2}{d_1^{\zeta_1}} \geq \frac{|g_2|^2}{d_2^{\zeta_2}}$ are as follows

$$\left(R_{D.1}^d, R_{D.2}^d\right) = \begin{pmatrix} W\log_2\left(1 + \mu_1\gamma_1|g_1|^2\right), \\ W\log_2\left(1 + \frac{\mu_2\gamma_2|g_2|^2}{\mu_1\gamma_2|g_2|^2+1}\right) \end{pmatrix}, \tag{5}$$

where $\gamma_i = \frac{P_{dl}}{W\sigma_0^2 d_i^{\zeta_i}}$, W is the system bandwidth, and μ_1, μ_2 are the power allocation coefficients of $\mathcal{S}_1$ and $\mathcal{S}_2$, respectively, in which $\mu_1 + \mu_2 = 1$, $\mu_1 < \mu_2$. On the other hand, when $\frac{|g_1|^2}{d_1^{\zeta_1}} < \frac{|g_2|^2}{d_2^{\zeta_2}}$, we get

$$\left(R_{D.1}^d, R_{D.2}^d\right) = \begin{pmatrix} W\log_2\left(1 + \frac{\mu_1'\gamma_1|g_1|^2}{\mu_2'\gamma_1|g_1|^2+1}\right), \\ W\log_2\left(1 + \mu_2'\gamma_2|g_2|^2\right) \end{pmatrix}, \tag{6}$$

where in this case the power allocation coefficients of $\mathcal{S}_1$ and $\mathcal{S}_2$ become μ_1' and μ_2', respectively, $\mu_1{}' + \mu_2{}' = 1$, $\mu_1' > \mu_2'$. Here, the values of power allocation coefficients are $\mu_1 < 0.5$, $\mu_2' < 0.5$, and $(\mu_1, \mu_2) \neq (\mu_1', \mu_2')$. A strategy for how to select these two fixed pairs of power levels to minimize the OOP is provided in Section V. Note that [27] is a sub-case with respect to our scheme with $\mu_1' = \mu_2$ and $\mu_2' = \mu_1$.

In downlink pairwise NOMA, there are two possible FDO schemes when disregarding the relationship between $\frac{|g_1|^2}{d_1^{\zeta_1}}$ and $\frac{|g_2|^2}{d_2^{\zeta_2}}$ as follows:

(a) FDO1: SIC is always performed at $\mathcal{S}_1$ and therefore the power allocated to $\mathcal{S}_2$ is larger, $\mu_1 < \mu_2$. This means that $\mathcal{S}_2$'s signal is decoded at $\mathcal{S}_1$ first, then removed by SIC to decode $\mathcal{S}_1$'s signal without interference from $\mathcal{S}_2$'s signal. At $\mathcal{S}_2$, the signal can be decoded directly by considering $\mathcal{S}_1$'s signal as interference. The achievable data rates of $\mathcal{S}_1$ and $\mathcal{S}_2$ in FDO1, $(R^d_{F1.1}, R^d_{F1.2})$, are the same as $(R^d_{D.1}, R^d_{D.2})$ when $\frac{|g_1|^2}{d_1^{\zeta_1}} \geq \frac{|g_2|^2}{d_2^{\zeta_2}}$. However, since $\mathcal{S}_1$ needs to decode $\mathcal{S}_2$'s message before SIC, there exists a rate of decoding $\mathcal{S}_2$'s signal at $\mathcal{S}_1$, i.e., $R_1^{SIC} = W\log_2(1 + \frac{\mu_2\gamma_1|g_1|^2}{\mu_1\gamma_1|g_1|^2+1})$.

(b) FDO2: SIC is always performed at $\mathcal{S}_2$ and the power allocated to $\mathcal{S}_1$ is bigger, $\mu_1' > \mu_2'$. In this case, $\mathcal{S}_1$'s signal is decoded at $\mathcal{S}_2$ first, then removed by SIC to decode $\mathcal{S}_2$'s signal without interference from $\mathcal{S}_1$'s signal. At $\mathcal{S}_1$, the signal can be decoded directly by considering $\mathcal{S}_2$'s signal as interference. The achievable data rates of $\mathcal{S}_1$ and $\mathcal{S}_2$ in FDO2, $(R^d_{F2.1}, R^d_{F2.2})$, are the same as $(R^d_{D.1}, R^d_{D.2})$ when $\frac{|g_1|^2}{d_1^{\zeta_1}} < \frac{|g_2|^2}{d_2^{\zeta_2}}$, and the rate of decoding $\mathcal{S}_1$'s signal at $\mathcal{S}_2$ is $R_2^{SIC} = W\log_2(1 + \frac{\mu_1'\gamma_2|g_2|^2}{\mu_2'\gamma_2|g_2|^2+1})$.

With $(\mu_1\gamma_1|g_1|^2 >> 1)$ and $(\mu_2'\gamma_2|g_2|^2 >> 1)$, in order to perform SIC at $\mathcal{S}_1$ and $\mathcal{S}_2$, the achievable rates for doing SIC have to exceed the respective target rates, i.e., $R_1^{SIC} \geq R^d_{2th}$ and $R_2^{SIC} \geq R^d_{1th}$. Therefore, we have

$$\mu_1 \leq \frac{1}{1 + A_2^d}, \tag{7}$$

$$\mu_2' \leq \frac{1}{1 + A_1^d}. \tag{8}$$

B. UPLINK PAIRWISE NOMA

For uplink pairwise NOMA, we propose a DDO scheme in which the signal with higher instantaneous normalized channel gain is decoded first, considering the other signal as noise. After performing SIC, the signal with lower instantaneous normalized channel gain can be decoded without interference. When the AP knows the CSIs, it decides on which signal is to be decoded first and which power levels are to be allocated to the respective source nodes. This decision is then communicated to the two source nodes before their transmissions. It should be noted that the two source nodes only switch between two fixed pairs of power levels in different time slots. For comparison, we not only consider the FPPA for this DDO scheme but also an ideal DPA which can be used if it is possible to inform the two source nodes about the dynamic pair of power levels calculated at the AP in each time slot.

1) FIXED PAIRWISE POWER ALLOCATION

With DDO-FPPA the achievable data rates for uplink pairwise NOMA with $\frac{|g_1|^2}{d_1^{\zeta_1}} \geq \frac{|g_2|^2}{d_2^{\zeta_2}}$ are as follows:

$$\left(R^u_{D.1}, R^u_{D.2}\right) = \begin{pmatrix} W\log_2\left(1 + \frac{\mu_1\gamma_{t1}|g_1|^2}{\mu_2\gamma_{t2}|g_2|^2+1}\right), \\ W\log_2\left(1 + \mu_2\gamma_{t2}|g_2|^2\right) \end{pmatrix}, \tag{9}$$

where $\gamma_{ti} = \frac{P_{ul}}{W\sigma_0^2 d_i^{\zeta_i}}$. However, when $\frac{|g_1|^2}{d_1^{\zeta_1}} < \frac{|g_2|^2}{d_2^{\zeta_2}}$, the data rates are

$$\left(R^u_{D.1}, R^u_{D.2}\right) = \begin{pmatrix} W\log_2\left(1 + \mu_1'\gamma_{t1}|g_1|^2\right), \\ W\log_2\left(1 + \frac{\mu_2'\gamma_{t2}|g_2|^2}{\mu_1'\gamma_{t1}|g_1|^2+1}\right) \end{pmatrix}. \tag{10}$$

Here, $(\mu_1, \mu_2) \neq (\mu_1', \mu_2')$, while $(\mu_1, \mu_2) = (\mu_1', \mu_2')$ was used in [25]–[27].

Similar to downlink pairwise NOMA, we can define two FDO schemes for uplink pairwise NOMA when the relationship between $\frac{|g_1|^2}{d_1^{\zeta_1}}$ and $\frac{|g_2|^2}{d_2^{\zeta_2}}$ is ignored:

(a) FDO1: First, $\mathcal{S}_1$'s signal is decoded by considering $\mathcal{S}_2$'s signal as interference and then removed by SIC to decode $\mathcal{S}_2$'s signal without interference from $\mathcal{S}_1$. The achievable data rates of $\mathcal{S}_1$ and $\mathcal{S}_2$ in FDO1, $(R^u_{F1.1}, R^u_{F1.2})$, are the same as $(R^u_{D.1}, R^u_{D.2})$ when $\frac{|g_1|^2}{d_1^{\zeta_1}} \geq \frac{|g_2|^2}{d_2^{\zeta_2}}$.

(b) FDO2: $\mathcal{S}_2$'s signal is decoded by considering $\mathcal{S}_1$'s signal as interference and then removed by SIC to decode $\mathcal{S}_1$'s signal without interference from $\mathcal{S}_2$. The achievable data rates of $\mathcal{S}_1$ and $\mathcal{S}_2$ in FDO2, $(R^u_{F2.1}, R^u_{F2.2})$, are the same as $(R^u_{D.1}, R^u_{D.2})$ when $\frac{|g_1|^2}{d_1^{\zeta_1}} < \frac{|g_2|^2}{d_2^{\zeta_2}}$.

Note that with $(\mu_2\gamma_{t2}|g_2|^2 >> 1)$ and $(\mu_1'\gamma_{t1}|g_1|^2 >> 1)$, and suppose that R^u_{ith} is the target rate at source node $\mathcal{S}_i$, in order to perform SIC at the AP we need $W\log_2(1 + \frac{\mu_1\gamma_{t1}|g_1|^2}{\mu_2\gamma_{t2}|g_2|^2+1}) \geq R^u_{1th}$ and $W\log_2(1 + \frac{\mu_2'\gamma_{t2}|g_2|^2}{\mu_1'\gamma_{t1}|g_1|^2+1}) \geq R^u_{2th}$. As a result, we have

$$\mu_1 \geq \frac{A_1^u}{1 + A_1^u}, \tag{11}$$

$$\mu_2' \geq \frac{A_2^u}{1 + A_2^u}. \tag{12}$$

2) IDEAL DYNAMIC POWER ALLOCATION

The power allocation for each source node is adjusted following the instantaneous channel conditions in each time slot. The two source nodes need to receive these power allocations before transmitting somehow. To successfully decode both signals at the AP, the achievable rates in (9) and (10) have to exceed the target rates, i.e., $R^u_{D.1} \geq R^u_{1th}$ and $R^u_{D.2} \geq R^u_{2th}$, where R^u_{1th} and R^u_{2th} are the target rates of $\mathcal{S}_1$ and $\mathcal{S}_2$, respectively. Define $A_1^u = 2^{\frac{R^u_{1th}}{W}} - 1$, $A_2^u = 2^{\frac{R^u_{2th}}{W}} - 1$, the minimum power levels needed for successful decoding are:

$\mu_1^{\min} = \frac{A_1^u(\gamma_{t2}|g_2|^2+1)}{\gamma_{t1}|g_1|^2+A_1^u\gamma_{t2}|g_2|^2}$, $\mu_2^{\min} = \frac{A_2^u}{\gamma_{t2}|g_2|^2}$, $\mu_1'^{\min} = \frac{A_1^u}{\gamma_{t1}|g_1|^2}$, and $\mu_2'^{\min} = \frac{A_2^u(\gamma_{t1}|g_1|^2+1)}{\gamma_{t2}|g_2|^2+A_2^u\gamma_{t1}|g_1|^2}$.

IV. OVERALL OUTAGE PROBABILITY ANALYSIS

In this section, we investigate the OOP for both uplink and downlink pairwise NOMA. The system experiences an outage when at least one of the two source nodes target a rate that is beyond its capacity. Hence, the OOP is defined differently for uplink and downlink pairwise NOMA. The closed-form expressions of the OOPs for all cases of decoding orders are derived based on the following theorem.

Theorem 1: Given two random variables $X \sim G(m_X, \frac{\gamma_X}{m_X})$ and $Y \sim G(m_Y, \frac{\gamma_Y}{m_Y})$ where m_X, m_Y are positive integers, the closed-form expression of the probability $p = \Pr\{(X \geq a) \cap (Y \geq bX + c)\}$, $(a \geq 0, b \geq 0, c \geq 0)$, can be derived as follows:

(a) $a \neq 0, b \neq 0, c = 0$:

$$p_a = \frac{\left(m_X\gamma_X^{-1}\right)^{m_X}}{\Gamma(m_X)} \sum_{i=0}^{m_Y-1} \frac{\left(m_Y\gamma_Y^{-1}b\right)^i \Gamma(m_X+i, \rho a)}{i!\rho^{m_X+i}}, \quad (13)$$

(b) $a = 0, b \neq 0, c = 0$:

$$p_b = \frac{\left(m_X\gamma_X^{-1}\right)^{m_X}}{\Gamma(m_X)} \sum_{i=0}^{m_Y-1} \frac{\left(m_Y\gamma_Y^{-1}b\right)^i \Gamma(m_X+i)}{i!\rho^{m_X+i}}, \quad (14)$$

(c) $a \neq 0, b \neq 0, c \neq 0$:

$$p_c = \frac{\left(m_X\gamma_1^{-1}\right)^{m_X} e^{-m_Y\gamma_Y^{-1}c}}{\Gamma(m_X)} \sum_{i=0}^{m_Y-1} \frac{\left(m_Y\gamma_Y^{-1}c\right)^i}{i!} \times \sum_{j=0}^{i} \left\{ \binom{i}{j} \left(\frac{b}{c}\right)^j \frac{\Gamma(m_X+j, \rho a)}{\rho^{m_X+j}} \right\}, \quad (15)$$

(d) $a = 0, b \neq 0, c \neq 0$:

$$p_d = \frac{\left(m_X\gamma_1^{-1}\right)^{m_X} e^{-m_Y\gamma_Y^{-1}c}}{\Gamma(m_X)} \sum_{i=0}^{m_Y-1} \frac{\left(m_Y\gamma_Y^{-1}c\right)^i}{i!} \times \sum_{j=0}^{i} \left\{ \binom{i}{j} \left(\frac{b}{c}\right)^j \frac{\Gamma(m_X+j)}{\rho^{m_X+j}} \right\}, \quad (16)$$

where $\rho = m_1\gamma_1^{-1} + m_2\gamma_2^{-1}b$. $\binom{n}{k} = \frac{n!}{k!(n-k)!}$ is the binomial coefficient. $\Gamma(m, \mu) = \int_\mu^\infty t^{m-1}e^{-\mu}dt$ and $\Gamma(m) = \int_0^\infty t^{m-1}e^{-t}dt$ are the upper incomplete Gamma function and Gamma function, respectively. Note that m_X and m_Y are integer.

Proof: See the Appendix. ∎

A. DOWNLINK PAIRWISE NOMA

The OOP for downlink pairwise NOMA is defined as follows:

$$P^d = \Pr\Big(\big(R_1 < R_{1th}^d\big) \cup \big(R_2 < R_{2th}^d\big) \cup \big(R^{SIC} < R_{th}^{SIC}\big)\Big), \quad (17)$$

where (R_1, R_2) are the achievable rates of $\mathcal{S}_1$ and $\mathcal{S}_2$, respectively. Depending on which node performing SIC, the pair (R^{SIC}, R_{th}^{SIC}) becomes (R_1^{SIC}, R_{2th}^d) when $\mathcal{S}_1$ is chosen for SIC and (R_2^{SIC}, R_{1th}^d) otherwise. Applying the De Morgan's law, we have

$$\begin{aligned} P^d &= 1 - \Pr\left(\begin{array}{c} \overline{\big(R_1 < R_{1th}^d\big)} \cap \overline{\big(R_2 < R_{2th}^d\big)} \\ \cap\big(R^{SIC} < R_{th}^{SIC}\big) \end{array}\right) \\ &= 1 - \Pr\left(\begin{array}{c} \big(R_1 \geq R_{1th}^d\big) \cap \big(R_2 \geq R_{2th}^d\big) \\ \cap\big(R^{SIC} \geq R_{th}^{SIC}\big) \end{array}\right). \end{aligned} \quad (18)$$

For the case of DDO-FPPA scheme, since SIC is always performed at node i whose $\frac{|g_i|^2}{d_i^\xi}$ is higher, the condition $R^{SIC} \geq R_{th}^{SIC}$ is always satisfied. Thus, the OOP can be simplified to

$$\begin{aligned} P_D^d &= 1 - \Pr\Big(\big(R_1 \geq R_{1th}^d\big) \cap \big(R_2 \geq R_{2th}^d\big)\Big) \\ &= 1 - (I_1 + I_2), \end{aligned} \quad (19)$$

where I_1 and I_2 are defined as follows:

$$I_1 = \Pr\left\{\begin{array}{c} \big(\mu_1 h_1^d \geq A_1^d\big) \\ \cap\left(\frac{\mu_2 h_2^d}{\mu_1 h_2^d + 1} \geq A_2^d\right) \\ \cap\big(h_1^d \geq h_2^d\big) \end{array}\right\} = \Pr\left\{\begin{array}{c} \big(h_1^d \geq b_0\big) \\ \cap\big(h_2^d \geq b_1\big) \\ \cap\big(h_1^d \geq h_2^d\big) \end{array}\right\}, \quad (20)$$

$$I_2 = \Pr\left\{\begin{array}{c} \left(\frac{\mu_1' h_1^d}{\mu_2' h_1^d + 1} \geq A_1^d\right) \\ \cap\big(\mu_2' h_2^d \geq A_2^d\big) \\ \cap\big(h_1^d < h_2^d\big) \end{array}\right\} = \Pr\left\{\begin{array}{c} \big(h_1^d \geq b_1'\big) \\ \cap\big(h_2^d \geq b_0'\big) \\ \cap\big(h_2^d > h_1^d\big) \end{array}\right\}, \quad (21)$$

where $h_i^d = \gamma_i|g_i|^2$, $A_i^d = 2^{\frac{R_{ith}^d}{W}} - 1$, $b_0 = \frac{A_1^d}{\mu_1}$, $b_1 = \frac{A_2^d}{\mu_2 - A_2^d\mu_1}$, $b_0' = \frac{A_2^d}{\mu_2'}$, $b_1' = \frac{A_1^d}{\mu_1' - A_1^d\mu_2'}$. Since g_i follows Nakagami-m fading, we have $h_i^d \sim G(m_i, \frac{\gamma_i}{m_i})$. From (20) and (21), we can see that the closed-form expression of I_i cannot be derived by directly applying Theorem 1. Therefore, we use Venn diagrams to separate I_i into some sub-cases. The probability I_1 can be depicted as the double-crossed areas in Fig. 3 and accordingly, can be calculated as

$$I_1 = \begin{cases} I_{1a} & \frac{A_1^d}{A_2^d + A_1^d(1+A_2^d)} \leq \mu_1 < \min\left(0.5, \frac{1}{1+A_2^d}\right) \\ I_{1b} & 0 < \mu_1 < \frac{A_1^d}{A_2^d + A_1^d(1+A_2^d)}, \end{cases} \quad (22)$$

in which I_{1a} and I_{1b} are given as

$$\begin{aligned} I_{1a} &= \Pr\Big\{\big(h_1^d \geq h_2^d\big) \cap \big(h_2^d \geq b_1\big)\Big\} \\ &= \frac{\left(m_2\gamma_2^{-1}\right)^{m_2}}{\Gamma(m_2)} \sum_{i=0}^{m_1-1} \frac{\left(m_1\gamma_1^{-1}\right)^i \Gamma(m_2+i, b_1 b_2)}{i! b_2^{m_2+i}}, \end{aligned} \quad (23)$$

$$\begin{aligned} I_{1b} &= \Pr\Big\{\big(h_1^d \geq b_0\big) \cap \big(b_0 > h_2^d \geq b_1\big)\Big\} \\ &\quad + \Pr\Big\{\big(h_1^d \geq h_2^d\big) \cap \big(h_2^d \geq b_0\big)\Big\} \\ &= \Pr\Big\{\big(h_1^d \geq b_0\big) \cap \big(h_2^d \geq b_1\big)\Big\} \end{aligned}$$

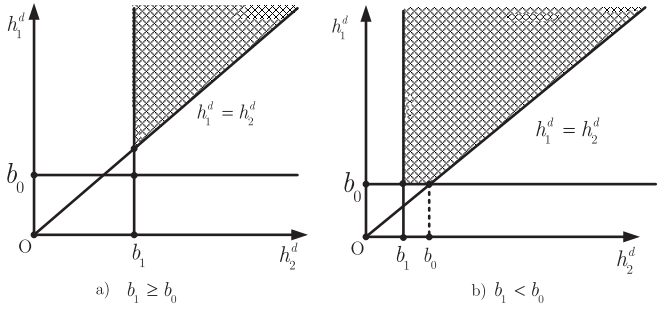

FIGURE 3. The Venn diagrams for calculating I_1 in downlink pairwise NOMA.

$$
\begin{aligned}
&- \Pr\left\{\left(h_1^d \geq b_0\right) \cap \left(h_2^d \geq b_0\right)\right\} \\
&+ \Pr\left\{\left(h_1^d \geq h_2^d\right) \cap \left(h_2^d \geq b_0\right)\right\} \\
&= \frac{\Gamma\left(m_1, m_1\gamma_1^{-1} b_0\right)}{\Gamma(m_1)} \\
&\quad \times \left[\frac{\Gamma\left(m_2, m_2\gamma_2^{-1} b_1\right)}{\Gamma(m_2)} - \frac{\Gamma\left(m_2, m_2\gamma_2^{-1} b_0\right)}{\Gamma(m_2)}\right] \\
&\quad + \frac{\left(m_2\gamma_2^{-1}\right)^{m_2}}{\Gamma(m_2)} \sum_{i=0}^{m_1-1} \frac{\left(m_1\gamma_1^{-1}\right)^i \Gamma(m_2+i, b_0 b_2)}{i! b_2^{m_2+i}}, \quad (24)
\end{aligned}
$$

where $b_2 = m_1\gamma_1^{-1} + m_2\gamma_2^{-1}$. Similarly, I_2 can be obtained as

$$
I_2 = \begin{cases} I_{2a} & \frac{A_2^d}{A_2^d(1+A_1^d)+A_1^d} \leq \mu_2' < \min\left(0.5, \frac{1}{1+A_1^d}\right) \\ I_{2b} & 0 < \mu_2' < \frac{A_2^d}{A_2^d(1+A_1^d)+A_1^d} \end{cases}, \quad (25)
$$

in which I_{2a} and I_{2b} are represented as follows:

$$
I_{2a} = \frac{\left(m_1\gamma_1^{-1}\right)^{m_1}}{\Gamma(m_1)} \sum_{i=0}^{m_2-1} \frac{\left(m_2\gamma_2^{-1}\right)^i \Gamma\left(m_1+i, b_1' b_2\right)}{i! b_2^{m_1+i}}, \quad (26)
$$

$$
\begin{aligned}
I_{2b} &= \frac{\left(m_1\gamma_1^{-1}\right)^{m_1}}{\Gamma(m_1)} \sum_{i=0}^{m_2-1} \frac{\left(m_2\gamma_2^{-1}\right)^i \Gamma\left(m_1+i, b_0' b_2\right)}{i! b_2^{m_1+i}} \\
&\quad + \frac{\Gamma\left(m_2, m_2\gamma_2^{-1} b_0'\right)}{\Gamma(m_2)} \\
&\quad \times \left[\frac{\Gamma\left(m_1, m_1\gamma_1^{-1} b_1'\right)}{\Gamma(m_1)} - \frac{\Gamma\left(m_1, m_1\gamma_1^{-1} b_0'\right)}{\Gamma(m_1)}\right]. \quad (27)
\end{aligned}
$$

Note that $\forall R_{1th}^d, R_{2th}^d$, we have $\frac{A_1^d}{A_2^d + A_1^d(1+A_2^d)} > 0$ and $\frac{A_2^d}{A_2^d(1+A_1^d)+A_1^d} > 0$, i.e., I_{1b} and I_{2b} always exist.

In an FDO scheme, however, (18) cannot be simplified to (19) since there exists a probability that $R^{SIC} < R_{th}^{SIC}$, and thus, SIC cannot be performed at the chosen node. For the case of FDO1, the OOP can be calculated as

$$
\begin{aligned}
P_{F1}^d &= 1 - \Pr\left\{\left(h_1^d \geq b_0\right) \cap \left(h_1^d \geq b_3\right) \cap \left(h_2^d \geq b_1\right)\right\} \\
&= 1 - \Pr\left(h_1^d \geq b_4\right) \Pr\left(h_2^d \geq b_1\right) \\
&= 1 - \frac{\Gamma\left(m_1, m_1\gamma_1^{-1} b_4\right)}{\Gamma(m_1)} \frac{\Gamma\left(m_2, m_2\gamma_2^{-1} b_1\right)}{\Gamma(m_2)}, \quad (28)
\end{aligned}
$$

where $b_3 = \frac{A_2^d}{\mu_2 - A_2^d\mu_1}$ and $b_4 = \max(b_0, b_3)$, and for the case of FDO2, the OOP can be calculated as

$$
\begin{aligned}
P_{F2}^d &= 1 - \Pr\left\{\left(h_1^d \geq b_1'\right) \cap \left(h_2^d \geq b_0'\right) \cap \left(h_2^d \geq b_3'\right)\right\} \\
&= 1 - \Pr\left(h_1^d \geq b_1'\right) \Pr\left(h_2^d \geq b_4'\right) \\
&= 1 - \frac{\Gamma\left(m_1, m_1\gamma_1^{-1} b_1'\right)}{\Gamma(m_1)} \frac{\Gamma\left(m_2, m_2\gamma_2^{-1} b_4'\right)}{\Gamma(m_2)}, \quad (29)
\end{aligned}
$$

where $b_3' = \frac{A_1^d}{\mu_1' - A_1^d\mu_2'}$ and $b_4' = \max(b_0', b_3')$.

B. UPLINK PAIRWISE NOMA

This subsection provides the calculation of the OOP for both FPPA and DPA in the context of DDO. As we mentioned above, the DDO-DPA scheme for uplink pairwise NOMA is impractical, however we still consider the OOP for this scheme for comparison purposes.

1) FIXED PAIRWISE POWER ALLOCATION

The system experiences an outage when the target rate pair and the sum rate are out of the capacity region. In other words, the OOP for uplink pairwise NOMA is defined as

$$
P^u = \Pr\left(\begin{array}{c}\left(R_1 < R_{1th}^u\right) \cup \left(R_2 < R_{2th}^u\right) \\ \cup\left(R_s < R_{1th}^u + R_{2th}^u\right)\end{array}\right), \quad (30)
$$

where $R_s = W\log_2(1 + \mu_1\gamma_{t1}|g_1|^2 + \mu_2\gamma_{t2}|g_2|^2)$ is the total sum rate. Note that the condition of sum rate $R_s \geq R_{1th}^u + R_{2th}^u$ is always satisfied when $R_1 \geq R_{1th}^u$ and $R_2 \geq R_{2th}^u$, and by applying the De Morgan's law, we have

$$
\begin{aligned}
P^u &= 1 - \Pr\left(\begin{array}{c}\overline{\left(R_1 < R_{1th}^u\right)} \cap \overline{\left(R_2 < R_{2th}^u\right)} \\ \cap\left(R_s < R_{1th}^u + R_{2th}^u\right)\end{array}\right) \\
&= 1 - \Pr\left(\begin{array}{c}\left(R_1 \geq R_{1th}^u\right) \cap \left(R_2 \geq R_{2th}^u\right) \\ \cap\left(R_s \geq R_{1th}^u + R_{2th}^u\right)\end{array}\right) \\
&= 1 - \Pr\left(\left(R_1 \geq R_{1th}^u\right) \cap \left(R_2 \geq R_{2th}^u\right)\right). \quad (31)
\end{aligned}
$$

The OOP for the case of DDO-FPPA scheme can be calculated as

$$
P_D^u = 1 - (I_3 + I_4), \quad (32)
$$

where I_3 and I_4 are given as

$$
\begin{aligned}
I_3 &= \Pr\left\{\left(\frac{\mu_1 h_1^u}{\mu_2 h_2^u + 1} \geq A_1^u\right) \cap \left(\mu_2 h_2^u \geq A_2^u\right) \cap \left(h_1^u \geq h_2^u\right)\right\} \\
&= \Pr\left\{\left(h_1^u \geq a_1 h_2^u + c_1\right) \cap \left(h_2^u \geq a_0\right) \cap \left(h_1^u \geq h_2^u\right)\right\}, \quad (33) \\
I_4 &= \Pr\left\{\left(\mu_1' h_1^u \geq A_1^u\right) \cap \left(\frac{\mu_2' h_2^u}{\mu_1' h_1^u + 1} \geq A_2^u\right) \cap \left(h_1^u < h_2^u\right)\right\} \\
&= \Pr\left\{\left(h_1^u \geq a_0'\right) \cap \left(h_2^u \geq a_1' h_1^u + c_1'\right) \cap \left(h_2^u > h_1^u\right)\right\}, \quad (34)
\end{aligned}
$$

where $h_i^u = \gamma_{ti}|g_i|^2$, $a_0 = \frac{A_2^u}{\mu_2}$, $a_1 = \frac{A_1^u\mu_2}{\mu_1}$, $c_1 = \frac{A_1^u}{\mu_1}$, $a_0' = \frac{A_1^u}{\mu_1'}$, $a_1' = \frac{A_2^u\mu_1'}{\mu_2'}$, $c_1' = \frac{A_2^u}{\mu_2'}$. Note that $h_i^u \sim G(m_i, \frac{\gamma_{ti}}{m_i})$, the

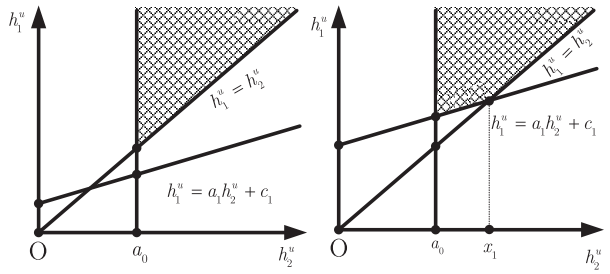

FIGURE 4. The Venn diagrams for calculating I_3 in uplink pairwise NOMA.

Venn diagrams in Fig. 4 are used to derive the closed-form expression of I_3 by applying the Theorem 1. Accordingly, I_3 can be calculated as

$$I_3 = \begin{cases} I_{3a} & \frac{A_1^u(1+A_2^u)}{A_2^u+A_1^u(1+A_2^u)} \leq \mu_1 < 1 \\ I_{3b} & \frac{A_1^u}{1+A_1^u} \leq \mu_1 < \frac{A_1^u(1+A_2^u)}{A_2^u+A_1^u(1+A_2^u)}, \end{cases} \tag{35}$$

where I_{3a} and I_{3b} are represented as

$$\begin{aligned} I_{3a} &= \Pr\left\{\left(h_1^u \geq h_2^u\right) \cap \left(h_2^u \geq a_0\right)\right\} \\ &= \frac{\left(m_2\gamma_{t2}^{-1}\right)^{m_2}}{\Gamma(m_2)} \sum_{i=0}^{m_1-1} \frac{\left(m_1\gamma_{t1}^{-1}\right)^i \Gamma(m_2+i, a_0 a_2)}{i! a_2^{m_2+i}}, \end{aligned} \tag{36}$$

$$\begin{aligned} I_{3b} &= \Pr\left\{\left(h_1^u \geq a_1 h_2^u + c_1\right) \cap \left(x_1 \geq h_2^u \geq a_0\right)\right\} \\ &\quad + \Pr\left\{\left(h_1^u \geq h_2^u\right) \cap \left(h_2^u \geq x_1\right)\right\} \\ &= \Pr\left\{\left(h_1^u \geq a_1 h_2^u + c_1\right) \cap \left(h_2^u \geq a_0\right)\right\} \\ &\quad - \Pr\left\{\left(h_1^u \geq a_1 h_2^u + c_1\right) \cap \left(h_2^u \geq x_1\right)\right\} \\ &\quad + \Pr\left\{\left(h_1^u \geq h_2^u\right) \cap \left(h_2^u \geq x_1\right)\right\} \\ &= \frac{\left(m_2\gamma_{t2}^{-1}\right)^{m_2} e^{-m_1\gamma_{t1}^{-1}c_1}}{\Gamma(m_2)} \sum_{i=0}^{m_1-1} \frac{\left(m_1\gamma_{t1}^{-1}c_1\right)^i}{i!} \\ &\quad \times \sum_{j=0}^{i} \left\{ \binom{i}{j} \left(\frac{a_1}{c_1}\right)^j \right. \\ &\quad \left. \times \left[\frac{\Gamma(m_2+j, a_0 a_3)}{a_3^{m_2+j}} - \frac{\Gamma(m_2+j, x_1 a_3)}{a_3^{m_2+j}} \right] \right\} \\ &\quad + \frac{\left(m_2\gamma_{t2}^{-1}\right)^{m_2}}{\Gamma(m_2)} \sum_{i=0}^{m_1-1} \frac{\left(m_1\gamma_{t1}^{-1}\right)^i \Gamma(m_2+i, x_1 a_2)}{i! a_2^{m_2+i}}, \end{aligned} \tag{37}$$

where $x_1 = \frac{c_1}{1-a_1}$, $a_2 = m_1\gamma_{t1}^{-1} + m_2\gamma_{t2}^{-1}$, $a_3 = m_2\gamma_{t2}^{-1} + m_1\gamma_{t1}^{-1}a_1$. Similarly, I_4 can be categorized into two cases as in (39) and (40):

$$I_4 = \begin{cases} I_{4a} & \frac{A_2^u(1+A_1)}{A_1^u+A_2^u(1+A_1^u)} \leq \mu_2' < 1 \\ I_{4b} & \frac{A_2^u}{1+A_2^u} \leq \mu_2' < \frac{A_2^u(1+A_1^u)}{A_1+A_2^u(1+A_1^u)}, \end{cases} \tag{38}$$

in which I_{4a} and I_{4b} can be obtained as follows:

$$I_{4a} = \frac{\left(m_1\gamma_{t1}^{-1}\right)^{m_1}}{\Gamma(m_1)} \sum_{i=0}^{m_2-1} \frac{\left(m_2\gamma_{t2}^{-1}\right)^i \Gamma\left(m_1+i, a_0' a_2\right)}{i! a_2^{m_1+i}}, \tag{39}$$

$$\begin{aligned} I_{4b} &= \frac{\left(m_1\gamma_{t1}^{-1}\right)^{m_1} e^{-m_2\gamma_{t2}^{-1}c_1'}}{\Gamma(m_1)} \sum_{i=0}^{m_2-1} \frac{\left(m_2\gamma_{t2}^{-1}c_1'\right)^i}{i!} \\ &\quad \times \sum_{j=0}^{i} \left\{ \binom{i}{j} \left(\frac{a_1'}{c_1'}\right)^j \right. \\ &\quad \left. \times \left[\frac{\Gamma\left(m_1+j, a_0' a_4\right)}{a_4^{m_1+j}} - \frac{\Gamma(m_1+j, x_2 a_4)}{a_4^{m_1+j}} \right] \right\} \\ &\quad + \frac{\left(m_1\gamma_{t1}^{-1}\right)^{m_1}}{\Gamma(m_1)} \sum_{i=0}^{m_2-1} \frac{\left(m_2\gamma_{t2}^{-1}\right)^i \Gamma(m_1+i, x_2 a_2)}{i! a_2^{m_1+i}}, \end{aligned} \tag{40}$$

where $x_2 = \frac{c_1'}{1-a_1'}$, $a_4 = m_2\gamma_{t2}^{-1}a_1' + m_1\gamma_{t1}^{-1}$.

The OOP for FDO1 scheme can be calculated as

$$\begin{aligned} P_{F1}^u &= 1 - \Pr\left\{\left(\frac{\mu_1 h_1^u}{\mu_2 h_2^u + 1} \geq A_1^u\right) \cap \left(h_2^u \geq \frac{A_2^u}{\mu_2}\right)\right\} \\ &= 1 - \Pr\left\{\left(h_1^u \geq a_1 h_2^u + c_1\right) \cap \left(h_2^u \geq a_0\right)\right\} \\ &= 1 - \frac{\left(m_2\gamma_{t2}^{-1}\right)^{m_2} e^{-m_1\gamma_{t1}^{-1}c_1}}{\Gamma(m_2)} \sum_{i=0}^{m_1-1} \frac{\left(m_1\gamma_{t1}^{-1}c_1\right)^i}{i!} \\ &\quad \times \sum_{j=0}^{i} \left\{ \binom{i}{j} \left(\frac{a_1}{c_1}\right)^j \frac{\Gamma(m_2+j, a_0 a_3)}{a_3^{m_2+j}} \right\}. \end{aligned} \tag{41}$$

The OOP for FDO2 scheme can be calculated as

$$\begin{aligned} P_{F2}^u &= 1 - \Pr\left\{\left(\mu_1 h_1^u \geq A_1^u\right) \cap \left(\frac{\mu_2 h_2^u}{\mu_1 h_1^u + 1} \geq A_2^u\right)\right\} \\ &= 1 - \Pr\left\{\left(h_2^u \geq a_1' h_1^u + c_1'\right) \cap \left(h_1^u \geq a_0'\right)\right\} \\ &= 1 - \frac{\left(m_1\gamma_{t1}^{-1}\right)^{m_1} e^{-m_2\gamma_{t2}^{-1}c_1'}}{\Gamma(m_1)} \sum_{i=0}^{m_2-1} \frac{\left(m_2\gamma_{t2}^{-1}c_1'\right)^i}{i!} \\ &\quad \times \sum_{j=0}^{i} \left\{ \binom{i}{j} \left(\frac{a_1'}{c_1'}\right)^j \frac{\Gamma\left(m_1+j, a_0' a_4\right)}{a_4^{m_1+j}} \right\}. \end{aligned} \tag{42}$$

2) IDEAL DYNAMIC POWER ALLOCATION

To correctly decode both source nodes' signals at the AP, the needed power does not exceed P_{ul}, i.e., $\mu_1^{\min} + \mu_2^{\min} \leq 1$ and ${\mu_1'}^{\min} + {\mu_2'}^{\min} \leq 1$. Therefore, the OOP for the DDO-DPA is defined as follow:

$$\begin{aligned} P_{DP}^u &= 1 - \Pr\left\{\left(\mu_1^{\min} + \mu_2^{\min} \leq 1\right) \cap \left(\frac{|g_1|^2}{d_1^{\zeta_1}} \geq \frac{|g_2|^2}{d_2^{\zeta_2}}\right)\right\} \\ &\quad - \Pr\left\{\left({\mu_1'}^{\min} + {\mu_2'}^{\min} \leq 1\right) \cap \left(\frac{|g_1|^2}{d_1^{\zeta_1}} < \frac{|g_2|^2}{d_2^{\zeta_2}}\right)\right\}. \end{aligned} \tag{43}$$

Algorithm 1 Finding Optimal Power Allocation Coefficients With $\mu_1 \neq \mu_2'$ in Downlink Pairwise NOMA

Input: R_{1th}, R_{2th} λ_1, λ_2, ζ_1, ζ_2, d_2, d_1, P_{dl}, σ_0^2, W.

Output: $\left(\mu_{1opt}, \mu'_{2opt}\right)$.

function main

Step 1: Find roots μ_{1c} in $\left(0, \frac{A_1^d}{A_2^d+A_1^d(1+A_2^d)}\right)$ and μ'_{2c} in $\left(0, \frac{A_2^d}{A_2^d(1+A_1^d)+A_1^d}\right)$ such that $\frac{\partial I_{1b}}{\partial \mu_1}(\mu_{1c}) = 0$ and $\frac{\partial I_{2b}}{\partial \mu'_2}(\mu'_{2c}) = 0$ $\lhd$ (63), (64);

Step 2: Find the optimal power allocation coefficients:

if (There exists no root in **Step 1**) **then**

$\mu_{1opt} = \frac{A_1^d}{A_2^d+A_1^d(1+A_2^d)}$;

$\mu'_{2opt} = \frac{A_2^d}{A_2^d+A_1^d(1+A_2^d)}$;

else

$\mu_{1opt} \longrightarrow \max\left(I_{1b}(\frac{A_1^d}{A_2^d+A_1^d(1+A_2^d)}), I_{1b}(\mu_{1c})\right)$;

$\mu'_{2opt} \longrightarrow \max\left(I_{2b}(\frac{A_2^d}{A_2^d+A_1^d(1+A_2^d)}), I_{2b}(\mu'_{2c})\right)$;

end if

Step 3: return $\left(\mu_{1opt}, \mu'_{2opt}\right)$.

end function

V. OPTIMAL POWER ALLOCATION

In this work, we aim to find the optimal fixed pairs of power allocations to minimize the OOP in both uplink and downlink pairwise NOMA. Combining the expressions of the OOPs as well as the ranges on μ_1 and μ'_2 in equations (19), (22), (25), (32), (35), and (38), we can formulate optimization problems for downlink and uplink respectively as follows:

$$\max_{\mu_1,\mu'_2} \quad I_1, I_2 \tag{44a}$$

$$\text{subject to:} \quad 0 < \mu_1 \leq \min\left(0.5, \frac{1}{1+A_2^d}\right) \tag{44b}$$

$$0 < \mu'_2 \leq \min\left(0.5, \frac{1}{1+A_1^d}\right) \tag{44c}$$

$$\max_{\mu_1,\mu'_2} \quad I_3, I_4 \tag{45a}$$

$$\text{subject to:} \quad \frac{A_1^u}{1+A_1^u} \leq \mu_1 < 1 \tag{45b}$$

$$\frac{A_2^u}{1+A_2^u} \leq \mu'_2 < 1 \tag{45c}$$

I_1, I_2, I_3, and I_4 always obtain a maximum value following the remark below.

Remark 1: The functions I_1, I_2, I_3, and I_4 obtain a maximum value either at the limit points or $\frac{\partial I_{1b}}{\partial \mu_1} = 0$, $\frac{\partial I_{2b}}{\partial \mu'_2} = 0$, $\frac{\partial I_{3b}}{\partial \mu_1} = 0$ and $\frac{\partial I_{4b}}{\partial \mu'_2} = 0$, respectively.

Algorithm 2 Finding Optimal Power Allocation Coefficients With $\mu_1 \neq \mu_2'$ in Uplink Pairwise NOMA

Input: R_{1th}, R_{2th} λ_1, λ_2, ζ_1, ζ_2, d_2, d_1, P_{ul}, σ_0^2, W.

Output: $\left(\mu_{1opt}, \mu'_{2opt}\right)$.

function main

Step 1: Find roots μ_{1c} in $\left(\frac{A_1^u}{1+A_1^u}, \frac{A_1^u(1+A_2^u)}{A_2^u+A_1^u(1+A_2^u)}\right)$ and μ'_{2c} in $\left(\frac{A_2^u}{1+A_2^u}, \frac{A_2^u(1+A_1^u)}{A_1^u+A_2^u(1+A_1^u)}\right)$ such that $\frac{\partial I_{3b}}{\partial \mu_1}(\mu_{1c}) = 0$ and $\frac{\partial I_{4b}}{\partial \mu'_2}(\mu'_{2c}) = 0$ $\lhd$ (65), as shown at the top of the p. 20, (66), as shown at the top of the p. 20;

Step 2: Find the optimal power allocation coefficients:

if (There exists no root in **Step 1**) **then**

$\mu_{1opt} \longrightarrow \max\begin{pmatrix} I_{3b}(\frac{A_1^u(1+A_2^u)}{A_2^u+A_1^u(1+A_2^u)}), \\ \lim\limits_{\mu_1 \to \frac{A_1^u}{1+A_1^u}} I_{3b} \end{pmatrix}$;

$\mu'_{2opt} \longrightarrow \max\begin{pmatrix} I_{4b}(\frac{A_2^u(1+A_1^u)}{A_2^u+A_1^u(1+A_2^u)}), \\ \lim\limits_{\mu_1 \to \frac{A_2^u}{1+A_2^u}} I_{4b} \end{pmatrix}$;

else

$\mu_{1opt} \longrightarrow \max\begin{pmatrix} I_{3b}(\frac{A_1^u(1+A_2^u)}{A_2^u+A_1^u(1+A_2^u)}), \\ I_{3b}(\mu_{1c}), \lim\limits_{\mu_1 \to \frac{A_1^u}{1+A_1^u}} I_{3b} \end{pmatrix}$;

$\mu'_{2opt} \longrightarrow \max\begin{pmatrix} I_{4b}(\frac{A_2^u(1+A_1^u)}{A_2^u+A_1^u(1+A_2^u)}), \\ I_{4b}(\mu'_{2c}), \lim\limits_{\mu_1 \to \frac{A_2^u}{1+A_2^u}} I_{4b} \end{pmatrix}$;

end if

Step 3: return $\left(\mu_{1opt}, \mu'_{2opt}\right)$.

end function

Proof: As presented in (44b), (44c), (45b), and (45c), to ensure the conditions for possible SIC at the receivers in both uplink and downlink pairwise NOMA, a range on the power allocation for each user is attained. Moreover, as illustrated in Figs. 3 and 4, since $b_0 > 0$, $b_1 > 0$, $a_0 > 0$, and $x_1 > 0$, we can conclude that I_1, I_2, I_3, and I_4 are continuous functions on their respective domains. Therefore, the right limit points of I_{1b}, I_{2b}, I_{3b}, and I_{4b} are also the left limit points of I_{1a}, I_{2a}, I_{3a}, and I_{4a}, respectively. Following the extreme value theorem [34], I_1, I_2, I_3, and I_4 always have maximum points over their domains. ■

To provide some insights into the OOP, we consider the case of $m_1 = m_2 = 1$, i.e., Rayleigh fading, and solve the optimization problems in (44), (45). By taking the partial derivatives of I_{1a} and I_{3a} with respect to μ_1, I_{2a} and I_{4a} with respect to μ'_2 we get:

$$\frac{\partial I_{1a}}{\partial \mu_1} = -\frac{A_2^d(A_2^d+1)e^{\frac{A_2^d\left(d_1^{\zeta_1}+d_2^{\zeta_2}\right)}{\gamma_2 d_2^{\zeta_2}(A_2^d\mu_1+\mu_1-1)}}}{\gamma_2(A_2^d\mu_1+\mu_1-1)^2} < 0. \tag{46}$$

$$\frac{\partial I_{2a}}{\partial \mu'_2} = -\frac{A_1^d(A_1^d+1)e^{\frac{A_1\left(d_1^{\zeta_1}+d_2^{\xi_2}\right)}{d1^{\zeta_1}\gamma_1\left(A_1^d\mu'_2+\mu'_2-1\right)}}}{\gamma_1\left(\mu'_2+A_1^d\mu'_2-1\right)^2} < 0. \tag{47}$$

$$\frac{\partial I_{3a}}{\partial \mu_1} = -\frac{A_2^u e^{-\frac{A_2^u\left(d_1^{\zeta_1}+d_2^{\zeta_2}\right)}{\gamma_{t2} d_2^{\zeta_2}(1-\mu_1)}}}{\gamma_{t2}(1-\mu_1)^2} < 0. \tag{48}$$

$$\frac{\partial I_{4a}}{\partial \mu_2'} = -\frac{A_1^u e^{-\frac{A_1^u\left(d_1^{\zeta_1}+d_2^{\zeta_2}\right)}{d_1^{\zeta_1}\gamma_{t1}(1-\mu_2')}}}{\gamma_{t1}(1-\mu_2')^2} < 0. \tag{49}$$

Thus, I_{1a}, I_{2a}, I_{3a}, and I_{4a} are decreasing functions on their respective subdomains in (22), (25), (35), and (38). In other words, I_{1a}, I_{2a}, I_{3a}, and I_{4a} attain maximums at the left limit points $\mu_1 = \frac{A_1^d}{A_2^d + A_1^d(1+A_2^d)}$, $\mu_2' = \frac{A_2^d}{A_2^d(1+A_1^d)+A_1^d}$, $\mu_1 = \frac{A_1^u(1+A_2^u)}{A_2^u+A_1^u(1+A_2^u)}$, and $\mu_2' = \frac{A_2^u(1+A_1^u)}{A_1^u+A_2^u(1+A_1^u)}$, respectively. On the other hand, I_{1b}, I_{2b}, I_{3b}, and I_{4b} can have maximums either at the critical points such that $\frac{\partial I_{1b}}{\partial \mu_1} = 0$, $\frac{\partial I_{2b}}{\partial \mu_2'} = 0$, $\frac{\partial I_{3b}}{\partial \mu_1} = 0$ and $\frac{\partial I_{4b}}{\partial \mu_2'} = 0$, or at the limit points. The left limit points of I_{1b}, I_{2b}, I_{3b}, and I_{4b} can be derived as

$$\lim_{\mu_1 \to 0} I_{1b} = 0, \tag{50}$$

$$\lim_{\mu_2' \to 0} I_{2b} = 0, \tag{51}$$

$$\lim_{\mu_1 \to \frac{A_1^u}{1+A_1^u}} I_{3b} = \frac{\gamma_{t1} e^{-\frac{A_2^u(1+A_1^u)}{\gamma_{t2}} - \frac{(A_2^u+1)(1+A_1^u)}{\gamma_{t1}}}}{\gamma_{t1}+\gamma_{t2}}, \tag{52}$$

$$\lim_{\mu_1 \to \frac{A_2^u}{1+A_2^u}} I_{4b} = \frac{\gamma_{t2} e^{-\frac{1+A_2^u}{\gamma_{t2}}} e^{-A_1^u(1+A_2^u)\left(\frac{1}{\gamma_{t1}}+\frac{1}{\gamma_{t2}}\right)}}{\gamma_{t2}+\gamma_{t1}}. \tag{53}$$

Eventually, the optimal points to minimize the OOPs for downlink and uplink can be achieved as shown in **Algorithm 1** and **Algorithm 2**, respectively.

Here the optimal power allocation coefficients to minimize the OOP for both source nodes are obtained and they should be $\mu_1 \neq \mu_1'$ and $\mu_2 \neq \mu_2'$. Note that $\mu_1 = \mu_1'$, $\mu_2 = \mu_2'$, and $\mu_1 > \mu_2$ are used in [25] when $\mathcal{S}_1$ is located in a better environment. However, we need to find roots two times to get the optimal power allocation coefficients (μ_{1opt}, μ_{2opt}) and $(\mu_{1opt}', \mu_{2opt}')$. To reduce the complexity and computational load at the AP, we propose a power allocation strategy with $\mu_1 = \mu_2'$, $\mu_2 = \mu_1'$ for both uplink and downlink pairwise NOMA. Now, the optimization problems in (44) and (45) are presented as follows:

$$\max_{\mu_1 = \mu_2'} \quad I_{12} = I_1 + I_2 \tag{54a}$$

$$\text{subject to:} \quad 0 < \mu_1 \leq \mu_0 \tag{54b}$$

$$\max_{\mu_1 = \mu_2'} \quad I_{34} = I_3 + I_4 \tag{55a}$$

$$\text{subject to:} \quad \mu_0' \leq \mu_1 < 1 \tag{55b}$$

Algorithm 3 Finding Optimal Power Allocation Coefficients With $\mu_1 = \mu_2'$ in Downlink Pairwise NOMA

Input: R_{1th}, R_{2th} λ_1, λ_2, ζ_1, ζ_2, d_2, d_1, P_{dl}, σ_0^2, W.
Output: $\mu_{1opt} = \mu_{2opt}'$.

1: **function** main
2: **Step 1:** Find roots μ_{1c} such that $\frac{\partial I_{12}}{\partial \mu_1}(\mu_{1c}) = 0$; Note that $\frac{\partial I_{12}}{\partial \mu_1}(\mu_{1c})$ can be obtained from (46), (47), (48), (49), (63), (64), (65), (66) following (56);
3: **Step 2:** Find the optimal power allocation coefficients:
4: **if** (There exists no root in **Step 1**) **then**
5: $\mu_{1opt} \rightarrow \max\left(\begin{matrix} I_{12}(\frac{A_1^d}{A_2^d+A_1^d(1+A_2^d)}), \\ I_{12}(\frac{A_2^d}{A_2^d+A_1^d(1+A_2^d)}) \end{matrix}\right)$;
6: **else**
7: $\mu_{1opt} \rightarrow \max\left(\begin{matrix} I_{12}(\frac{A_2^d}{A_2^d+A_1^d(1+A_2^d)}), I_{12}(\mu_{1c}), \\ I_{12}(\frac{A_1^d}{A_2^d+A_1^d(1+A_2^d)}) \end{matrix}\right)$;
8: **end if**
9: **Step 3: return** $\mu_{1opt} = \mu_{2opt}'$.
10: **end function**

where $\mu_0 = \min(0.5, \frac{1}{1+A_2^d}, \frac{1}{1+A_1^d})$, $\mu_0' = \max(\frac{A_2^u}{1+A_2^u}, \frac{A_1^u}{1+A_1^u})$. Here, the function I_{12} and I_{34} can be represented as follows:

$$I_{12} = \begin{cases} I_{1a} + I_{2a} \left(\frac{A_1^d}{A_2+A_1(1+A_2)} \leq \mu_1 \leq \mu_0; R_{1th}^d \geq R_{2th}^d\right) \\ \quad \vee\left(\frac{A_2^d}{A_2+A_1(1+A_2)} \leq \mu_1 \leq \mu_0; R_{1th}^d < R_{2th}^d\right), \\ I_{1b} + I_{2b} \left(0 < \mu_1 < \frac{A_2^d}{A_2+A_1(1+A_2)}; R_{1th}^d \geq R_{2th}^d\right) \\ \quad \vee\left(0 < \mu_1 < \frac{A_1^d}{A_2+A_1(1+A_2)}; R_{1th}^d < R_{2th}^d\right), \\ I_{1b} + I_{2a} \left(\frac{A_2^d}{A_2+A_1(1+A_2)} \leq \mu_1 < \frac{A_1^d}{A_2+A_1(1+A_2)}; R_{1th}^d \geq R_{2th}^d\right), \\ I_{1a} + I_{2b} \left(\frac{A_1^d}{A_2+A_1(1+A_2)} \leq \mu_1 < \frac{A_2^d}{A_2+A_1(1+A_2)}; R_{1th}^d < R_{2th}^d\right). \end{cases} \tag{56}$$

$$I_{34} = \begin{cases} I_{3a} + I_{4a} \left(\frac{A_1^u(1+A_2^u)}{A_2^u+A_1^u(1+A_2^u)} \leq \mu_1 < 1; R_{1th}^u \geq R_{2th}^u\right) \\ \quad \vee\left(\frac{A_2^u(1+A_1^u)}{A_2^u+A_1^u(1+A_2^u)} \leq \mu_1 < 1; R_{1th}^u < R_{2th}^u\right), \\ I_{3b} + I_{4b} \left(\mu_0' \leq \mu_1 < \frac{A_2^u(1+A_1^u)}{A_2^u+A_1^u(1+A_2^u)}; R_{1th}^u \geq R_{2th}^u\right) \\ \quad \vee\left(\mu_0' \leq \mu_1 < \frac{A_1^u(1+A_2^u)}{A_2^u+A_1^u(1+A_2^u)}; R_{1th}^u < R_{2th}^u\right), \\ I_{3b} + I_{4a} \left(\frac{A_2(1+A_1)}{A_2+A_1(1+A_2)} \leq \mu_1 < \frac{A_1(1+A_2)}{A_2+A_1(1+A_2)}; R_{1th}^u \geq R_{2th}^u\right) \\ I_{3a} + I_{4b} \left(\frac{A_1(1+A_2)}{A_2+A_1(1+A_2)} \leq \mu_1 < \frac{A_2(1+A_1)}{A_2+A_1(1+A_2)}; R_{1th}^u < R_{2th}^u\right) \end{cases} \tag{57}$$

Then, using the same approach as **Remark 1**, we can find the optimal power allocation factors $\mu_{1opt} = \mu_{2opt}'$ in both downlink and uplink pairwise NOMA by using **Algorithm 3** and **Algorithm 4**. Note that the complexity of Algorithms 1–4 depends on the method used for finding the roots at step 1 in these algorithms. Various methods for root-finding exist such

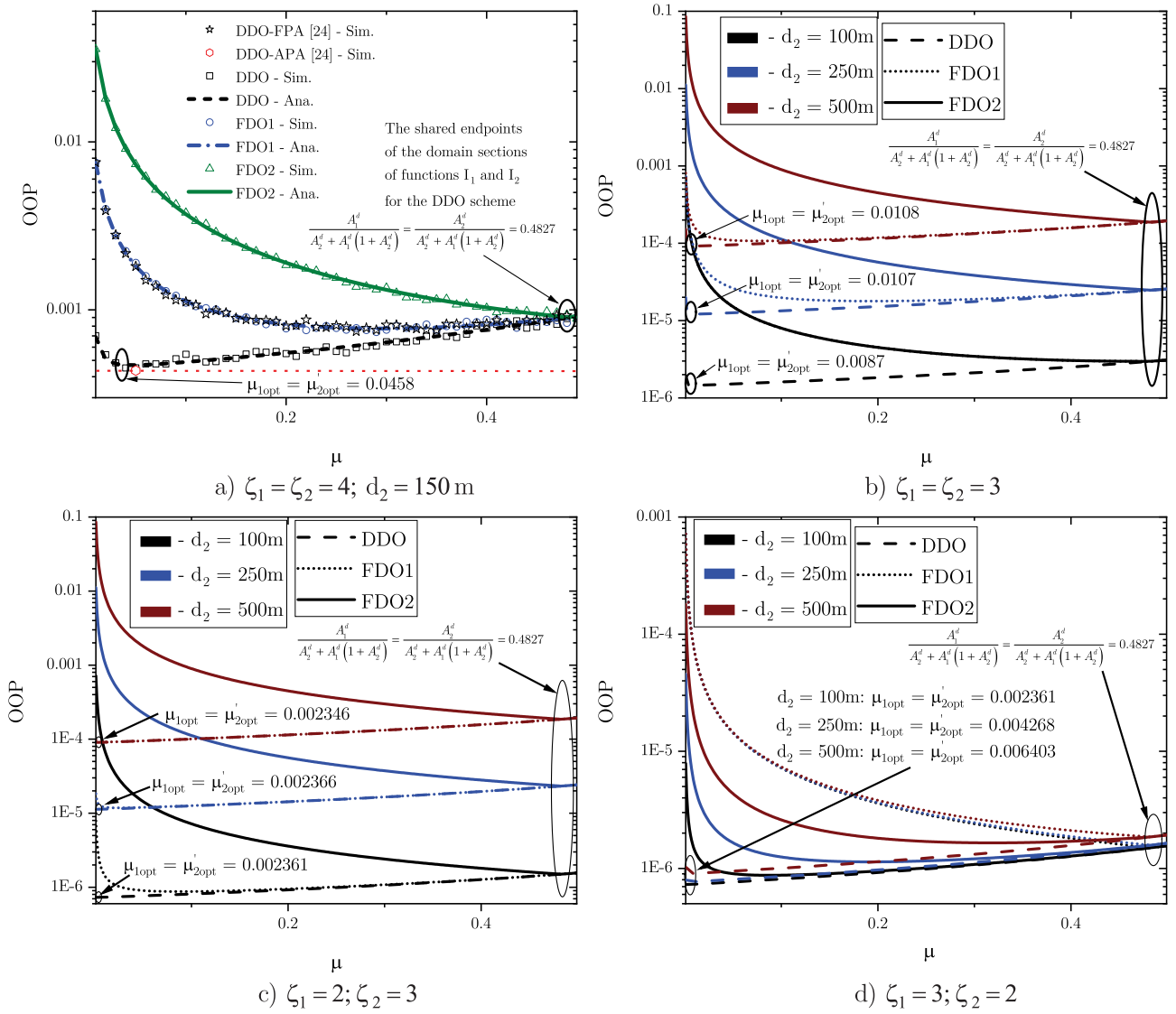

FIGURE 5. The OOP versus μ_1 for the downlink pairwise NOMA with $d_1 = 100$m, $R_{1th} = R_{2th} = 0.1$ bps.

as Bisection, Newton-Raphson, Secant, supported by different tools, e.g., Mathematica, MATLAB [35], [36]. In [35], [37], [38], a comparison in terms of convergence speed or performance (including both cost and speed of convergence) among the methods Bisection, Newton Raphson, Regula Falsi, Secant, and Fixed Point Iteration was studied using different tools, such as MATLAB, Mathematica, and manual computation. The results show that Secant method is the most effective in terms of performance, while Newton Raphson method is the most effective in terms of convergence speed [38, Tab. 6]. Another important thing is the number of necessary iterations for each method. In fact, this number depends on a range of parameters, e.g., error tolerance, initial approximation [35]. Moreover, we consider fixed power allocation strategies, in which the optimal power levels stay the same unless the channel distributions change. Thus, Algorithms 1–4 will be run once at the beginning as long as the channels keep following the same distributions.

VI. NUMERICAL RESULTS

In this section we present numerical results for the OOP of the considered system and elaborate on the performance of different decoding orders and power allocation strategies. The following system parameters are used: $W = 1$ Hz, $d_1 = 100$m, $P_{dl} = 10$W, $P_{ul} = 1$W, $m_1 = m_2 = 1$ except for Figs. 6, 10, 12, 16, and $\sigma_0^2 = 10^{-10}$W/Hz [39]. To check the correctness of the analysis in the previous section, we also perform computer simulations using MATLAB. In particular, for each considered OOP we first generate 10^7 samples of the channel gains following a Gamma distribution and then check the outage conditions as defined in (17), (30), and (43). The simulation results of the OOPs are then achieved by

Algorithm 4 Finding Optimal Power Allocation Coefficients With $\mu_1 = \mu_2'$ in Uplink Pairwise NOMA

Input: R_{1th}, R_{2th} λ_1, λ_2, ζ_1, ζ_2, d_2, d_1, P_{ul}, σ_0^2, W.
Output: $\mu_{1opt} = \mu'_{2opt}$.

1: **function** main
2: **Step 1:** Find roots μ_{1c} such that $\frac{\partial I_{34}}{\partial \mu_1}(\mu_{1c}) = 0$; Note that $\frac{\partial I_{34}}{\partial \mu_1}(\mu_{1c})$ can be obtained from (46), (47), (48), (49), (63), (64), (65), (66) following (57);
3: **Step 2:** Find the optimal power allocation coefficients:
4: **if** (There exists no root in **Step 1**) **then**
5: $$\mu_{1opt} \longrightarrow \max\begin{pmatrix} I_{34}(\frac{A_2^u(1+A_1^u)}{A_2^u+A_1^u(1+A_2^u)}), \\ \lim_{\mu_1\to\mu_0'} I_{34}, \\ I_{34}(\frac{A_1^u(1+A_2^u)}{A_2^u+A_1^u(1+A_2^u)}) \end{pmatrix};$$
6: **else**
7: $$\mu_{1opt} \longrightarrow \max\begin{pmatrix} I_{34}(\frac{A_2^u(1+A_1^u)}{A_2^u+A_1^u(1+A_2^u)}), \\ I_{34}(\mu_{1c}), \lim_{\mu_1\to\mu_0'} I_{34}, \\ I_{34}(\frac{A_1^u(1+A_2^u)}{A_2^u+A_1^u(1+A_2^u)}) \end{pmatrix};$$
8: **end if**
9: **Step 3: return** $\mu_{1opt} = \mu'_{2opt}$.
10: **end function**

taking the average of all outage events across 10^7 samples. We conclude the section by discussing the impact of different parameters on the OOP and how this should affect the power allocation strategy.

A. DOWNLINK PAIRWISE NOMA

Figs. 5 and 6 show the effect of the power allocation coefficient μ_1 on the OOP for all types of decoding orders in different environments and for varying locations of $\mathcal{S}_2$. Here we consider $\mu_1 = \mu_2' = \mu$ for the DDO-FPPA scheme, $\mu_1 = \mu$ for the FDO1 scheme, as well as $\mu_2' = \mu$ for the FDO2 scheme. Note that the range of both μ_1 and μ_2' in (22) and (25) is (0, 0.5). First, in Figs. 5a and 6 it is shown that simulation and analytical results match very well, and thus in Figs. 5b, 5c, and 5d we merely show the analytical results. Further, it can be seen from the Fig. 5a that the OOP using DDO-DPA is a bit better than our proposed scheme, while the OOP for DDO-FPA is close to that for the FDO1 scheme. However, we can also see that the OOP of our proposed scheme is better than all glsfo, Figs. 5b–d. Note that the OOP for FDO1 is the same as that for FDO2 with $d_2 = d_1 = 100$m and $\zeta_1 = \zeta_2 = 3$ in Fig. 5b due to the fact that $p_{RO} = 0.5$ in this case. Using **Algorithm 3**, we can find the optimal value of $\mu_{1opt} = \mu'_{2opt}$ to minimize the OOP. The shared endpoints of the domain sections of functions I_1 and I_2 are also shown in the figure, in which I_1 and I_2 are continuous functions. The OOPs for all types of decoding order increase significantly when the distance between the AP and $\mathcal{S}_2$ increases due to a higher path-loss. In general, when μ is very small, the OOP for all types of decoding orders decreases significantly as μ goes up. This is because

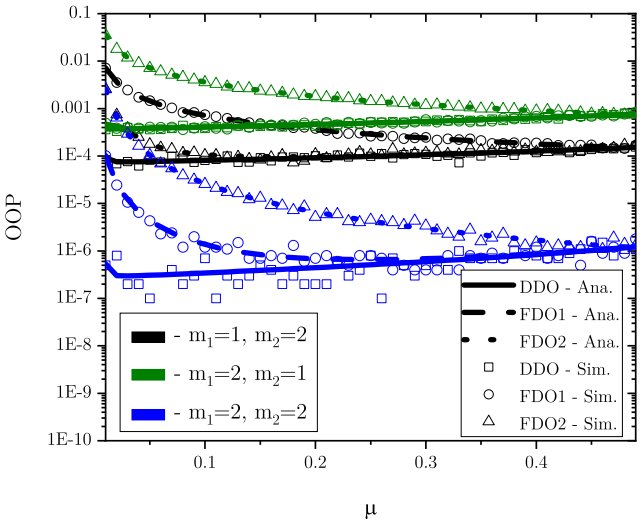

FIGURE 6. The OOP versus μ_1 for the downlink pairwise NOMA with $d_1 = 100$m, $\zeta_1 = \zeta_2 = 4$, $R_{1th} = R_{2th} = 0.1$ bps with different shape factors.

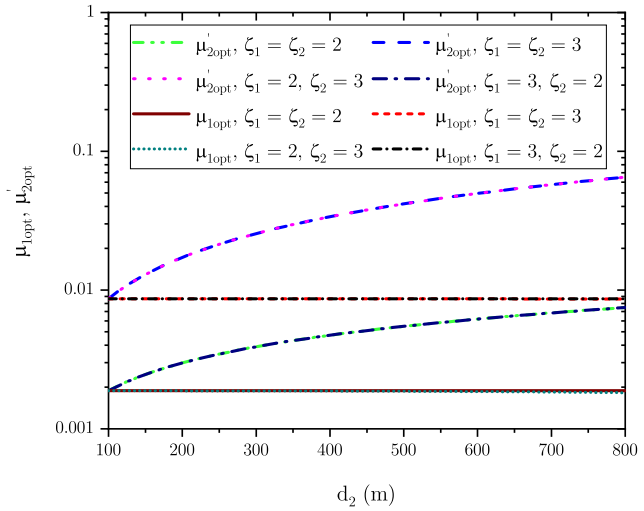

FIGURE 7. The μ_{1opt} and μ'_{2opt} versus d_2 for the downlink pairwise NOMA with $d_1 = 100$m using Algorithm 1 with $R_{1th} = R_{2th} = 0.1$ bps.

an increase of μ in this interval can improve the probability of successfully decoding at the user that is allocated a smaller power level. Increasing μ further, the OOP for the FDO2 scheme continues to decrease, while the OOP for the FDO1 scheme first goes down sharper and then slightly goes up as shown in Figs. 5a, b, c. The reason is that in these scenarios $\mathcal{S}_1$ experiences a better environment with $\zeta_1 \leq \zeta_2$, thus $\mathcal{S}_2$ needs more power to deal with higher path-loss. We can see clearly that the OOP for the FDO1 scheme is better than that of the FDO2 scheme for $\zeta_1 \leq \zeta_2$. On the other hand, when $\zeta_1 > \zeta_2$ in Fig. 5d, the FDO1 scheme is better.

Fig. 7 illustrates how the optimal power allocation for the DDO-FPPA scheme calculated using **Algorithm 1** changes in accordance with the distance between the AP and $\mathcal{S}_2$. In general, μ_{1opt} reduces very slightly with an increase of d_2. The reason is that significantly increasing the power allocated to $\mathcal{S}_2$ can escalate the probability of unsuccessfully

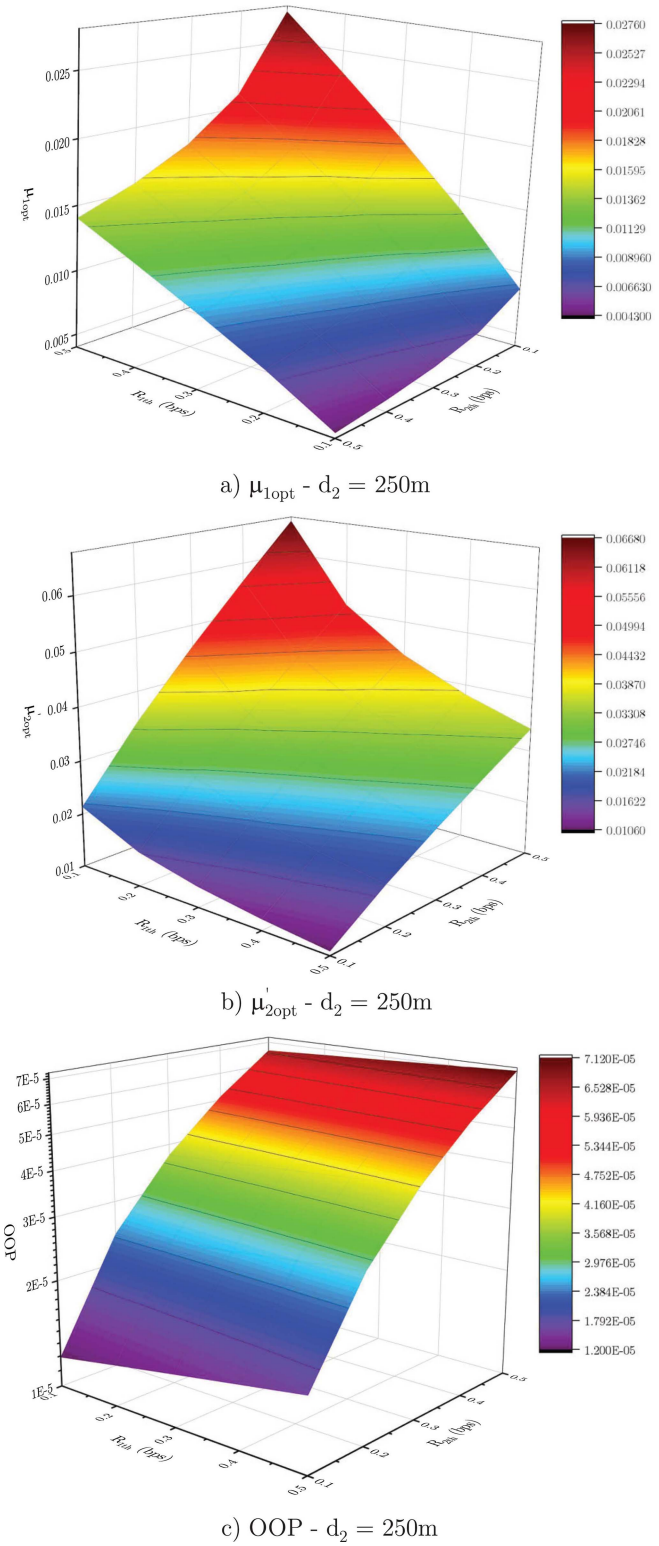

FIGURE 8. The OOP versus R_{1th} and R_{2th} for the downlink pairwise NOMA with $d_1 = 100$m using Algorithm 1 with $\zeta_1 = \zeta_2 = 3$.

decoding $\mathcal{S}_1$'s signal after $\mathcal{S}_2$'s signal is removed by SIC at $\mathcal{S}_1$. In contrast, μ'_{2opt} goes up significantly. This is because $\mathcal{S}_2$ needs more power to successfully decode its own signal after SIC at $\mathcal{S}_2$ when $\mathcal{S}_2$ experiences a higher path-loss.

Fig. 8 depicts how optimal power allocation coefficients for both users change following the target rates R_{1th}, R_{2th}, as well as the relationship between the OOP versus the target rates of the two users using the optimal power allocation with $d_2 = 250$m. From the figures, we have the following observations:

- In Fig. 8a, while the optimal power allocation coefficient μ_{1opt} goes up with an increase of R_{1th}, this coefficient decreases when R_{2th} rises. This is because SIC is performed at $\mathcal{S}_1$ and $\mathcal{S}_2$ is located farther away from the AP as compared to $\mathcal{S}_1$, thus $\mathcal{S}_2$ requires more power not only to overcome the higher path-loss but also to achieve a higher target rate R_{2th}.
- We can see a different phenomenon in Fig. 8b where μ'_{2opt} goes up dramatically when R_{2th} increases, while this optimal power factor decreases slightly with an increase of R_{1th}. In this case, the SIC unit is performed at $\mathcal{S}_2$. As a result, $\mathcal{S}_2$ needs more power to reduce the probability of unsuccessfully decoding its signal after SIC.
- In terms of reliability, the OOP increases significantly when $\mathcal{S}_2$ requires a higher target rate. In contrast, this probability grows slightly with an increase of R_{1th}. Consequently, it is better to choose two nodes for downlink pairwise NOMA with $R_{1th} \geq R_{2th}$ to improve the reliability.

Next, Figs. 9 and 10 illustrate how the path-loss exponents ζ_1, ζ_2, as well as d_2, ($d_2 \geq d_1$, $d_1 = 100$m) affect the OOP. Here, we also consider $\mu'_1 = \mu_2$ and $\mu'_2 = \mu_1$. Firstly, we can see in Figs. 9a and 10 that the analytical calculations and simulation results match, which demonstrates the accuracy of the analyses. Thus in Figs. 9b, 9c, and 9d only analytical results are shown. We investigate at different power allocation coefficients when the channels between the AP and $\mathcal{S}_i$ have the same or different path-loss exponents. Similar to as it was observed in Fig. 5, from these figures we can see that in terms of OOP, the DDO-FPPA scheme always performs the best, while the performance of the FDO1 scheme approaches that of the DDO-FPPA when $d_2 \gg d_1$ since then $p_{RO} \approx 1$. In general, the longer is the distance between the AP and $\mathcal{S}_2$, the higher are the OOPs for all considered schemes, due to the increase in path-loss. Furthermore, increasing μ_1 results in a degradation of the communication reliability as $\mathcal{S}_2$ needs more power to overcome the effect of stronger path-loss. With $\zeta_1 \leq \zeta_2$, as in Figs. 9b and 9c, the OOPs for all types of decoding orders go up rapidly as d_2 increases and FDO1 always performs better than FDO2. In contrast, the OOPs increase slightly for the case of $\zeta_1 > \zeta_2$ in Fig. 9d, since $\mathcal{S}_2$'s received power degrades slower over distance. Moreover, when $\zeta_1 > \zeta_2$ and the two users are close to the AP, FDO2 performs better than FDO1 since $\mathcal{S}_2$ has a better normalized channel gain, even if $d_2 > d_1$. We also investigate the optimal power allocation for the proposed DDO scheme with both **Algorithm 1** and **Algorithm 3** in Figs. 9b, c, d. We can see very subtle differences between these two optimal results. Therefore, in order

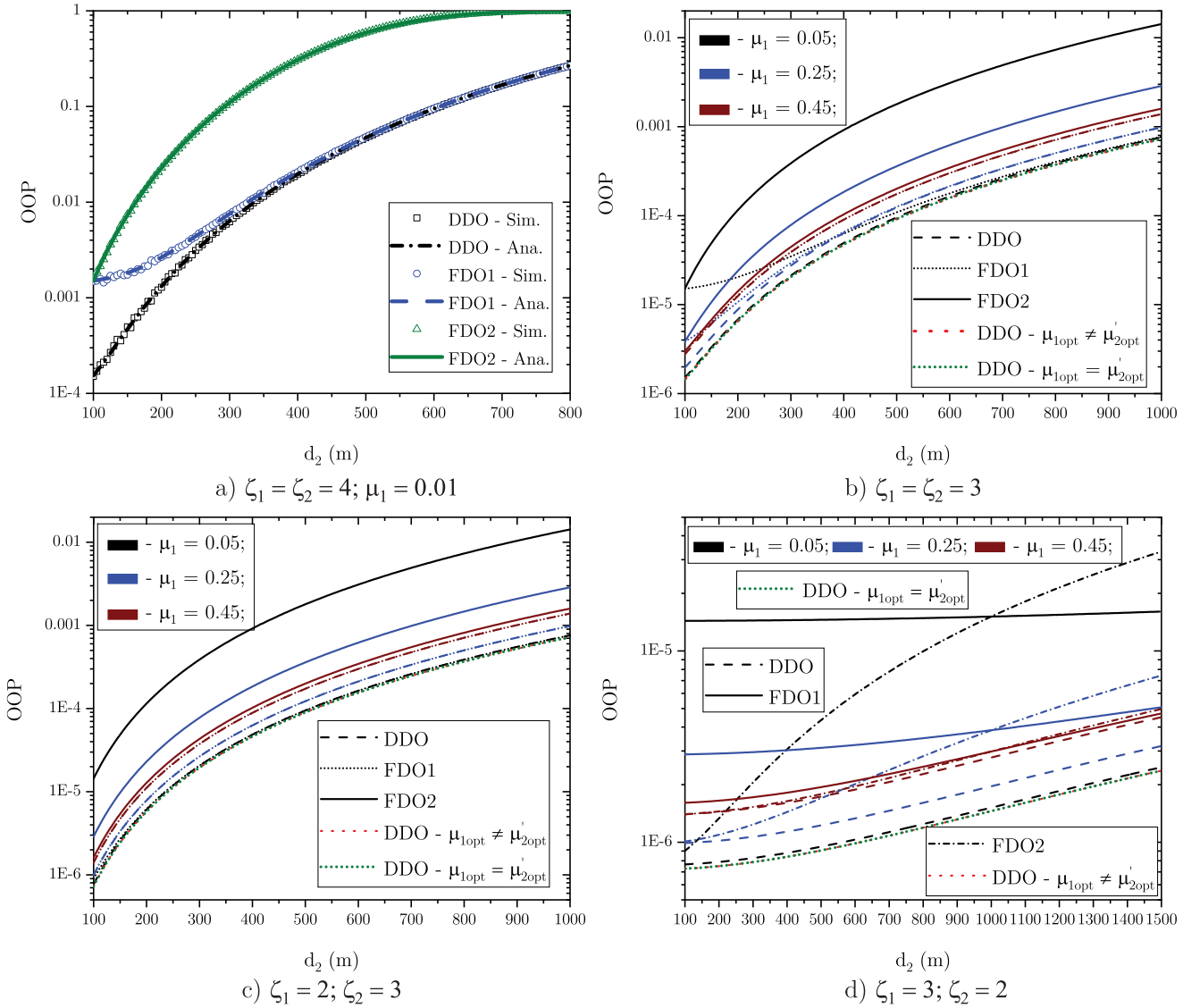

FIGURE 9. The OOP versus d_2 for the downlink pairwise NOMA with $d_1 = 100$m, $d_2 \geq d_1$, $R_{1th} = R_{2th} = 0.1$ bps.

to reduce the complexity and computational load at the AP, we only need to find the optimal power allocation factors $\mu_1 = \mu_2'$ following **Algorithm 3**. In addition, increasing μ_1 such that $\mu_1 = \mu_2' < 0.5$ in Figs. 9b, c, d degrades the OOP for the proposed DDO scheme to only a limited extent. This means that the power allocation does not affect much on the communication reliability in terms of OOP when the proposed DDO scheme is used.

B. UPLINK PAIRWISE NOMA

Figs. 11 and 12 illustrate how the power allocation affects the OOP for all types of decoding orders in different environments at $d_2 = 200$m. Note that the range of μ_1 and μ_2' according to (35), (38) is [0.067,1) in this case. We compare with the DDO scheme in [25] in which the source node with lower path-loss (stronger source node) is assigned more power than the other source node experiencing higher path-loss (weaker source node). Here the power allocation strategy of our proposed DDO scheme is more flexible, we thus consider $\mu_1 = \mu_2' = \mu$ with $\mu < 0.5$ and $\mu_1 = \mu_2' = 1 - \mu$ with $\mu \geq 0.5$ so that more power is always allocated to the weaker source node. Meanwhile, $\mu_1 = \mu_1' = \mu$ is used for both FDO schemes. We can see that the analyses and the simulations match very well, Figs. 11a and 12. Here the DDO scheme using the power allocation strategy in [25] is better than both FDO schemes but worse than our proposed DDO scheme, i.e., with fixed power levels our proposed DDO performs best in terms of OOP in all considered environments. In Fig. 11a, we can see that the OOP using a DDO-DPA is not much better than that for the DDO-FPPA scheme, while the DDO-DPA scheme is much more complex compared to the DDO-FPPA scheme as explained in Section I. Moreover, with the DDO-FPPA scheme, we can find the optimal power allocation for both

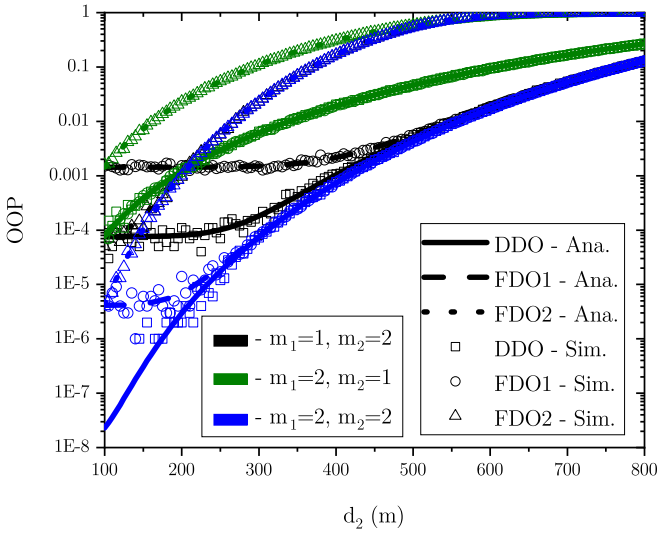

FIGURE 10. The OOP versus d_2 for the downlink pairwise NOMA with $d_1 = 100$m, $\zeta_1 = \zeta_2 = 4$, $R_{1th} = R_{2th} = 0.1$ bps with different shape factors.

source nodes using the **Algorithm 4**. In addition, we have the following observations:

- The OOP for the FDO1 scheme decreases significantly due to less interference from $\mathcal{S}_2$ in decoding $\mathcal{S}_1$'s signal, and then goes up with an increase of the power allocated to $\mathcal{S}_1$, Figs. 11a, b, c. The reason is that increasing μ_1 also reduces the power allocated to $\mathcal{S}_2$, thus increases the probability of unsuccessfully decoding $\mathcal{S}_2$'s signal, and then the OOP for the FDO1 scheme increases. Especially, the OOP for the FDO1 scheme is very high at smaller values of μ_1 and then decreases slightly when increasing μ in Fig. 11d due to the fact that $\mathcal{S}_1$ is located in a worse environment than $\mathcal{S}_2$, thus the AP can hardly decode $\mathcal{S}_1$'s signal with the interference from $\mathcal{S}_2$.
- Next, the OOP for the FDO2 scheme usually increases significantly, even reaches approximately 1 with $\zeta_2 > \zeta_1$, when μ_1 increases, due to the fact that $\mathcal{S}_2$ needs more power to overcome a higher path-loss. In most cases, the OOP for the FDO2 scheme is worse than that for the FDO1 scheme as $p_{RO} \geq 0.5$ with $\zeta_2 \geq \zeta_1$ and $d_2 \geq d_1$. In contrast, in Fig. 11d, since $p_{RO} < 0.5$, the OOP for FDO2 is much better than that for FDO1 as $\mathcal{S}_2$ is located in the better environment.
- In Fig. 11, the best value of μ_1 for the DDO scheme in [25] is 0.5. However, the OOP for this scheme is worse than that for our proposed DDO scheme. This is because of the power allocation strategy in [25] in which the weaker source node always performs worse as it is allocated less power.

Fig. 13 represents the optimal power allocation factors as functions of distance between the AP and $\mathcal{S}_2$, calculated using **Algorithm 2**. It can be seen from the figure that μ_{1opt} reduces slightly with an increase of d_2 for $\mathcal{S}_2$ getting more power to overcome a higher path-loss. In contrast, μ'_{2opt} goes up significantly to deal with interference from $\mathcal{S}_1$ as well as higher path-loss.

Fig. 14 shows the effect of the target rates R_{1th} and R_{2th} on the optimal power allocation coefficients as well as on the OOP. We can see the following:

- When R_{1th} increases, the optimal power allocated to $\mathcal{S}_1$ when it is chosen to perform SIC rises significantly as shown in Fig. 14a. However, reducing μ_1 does not help much to achieve higher R_{2th} with optimal OOP. The reason is that the AP first needs to perform SIC on $\mathcal{S}_1$'s signal, but μ_1 is already small, thus reducing μ_1 further will degrade the OOP. Furthermore, a high power allocation factor for $\mathcal{S}_1$ can help to increase the probability of successfully decoding $\mathcal{S}_1$'s signal.
- In contrast, an increase of R_{2th} leads to a significant growth of μ'_{2opt}, Fig. 14b, to achieve the optimal probability of successfully decoding both signals when $\mathcal{S}_2$ is chosen to perform SIC. Moreover, since $\mathcal{S}_2$'s signal is decoded first, when R_{1th} increases, it is allowed for only a slight increase of power allocated to $\mathcal{S}_1$ to achieve the optimal OOP.
- In general, increasing R_{1th} and/or R_{2th} results in a reduction of communication reliability. However, the OOP goes up dramatically when R_{2th} rises. Similar to downlink pairwise NOMA, $R_{2th} \leq R_{1th}$ is a good criteria to make a pair of NOMA source nodes in terms of reliability.

Figs. 15 and 16 show the OOP for uplink pairwise NOMA as a function of the distance between the AP and $\mathcal{S}_2$ in different environments for all cases of decoding orders. Similar to the downlink scenario, we can see from Figs. 15a and 16 that the calculations for uplink pairwise NOMA match the simulation results, and that the OOPs when using our proposed DDO are always better than FDOs. Here, $\mu_1 = \mu'_2 = 0.2$ means that the weaker source node is always assigned more power to overcome a higher path-loss. On the other hand, the OOP when using the power allocation strategy in [25] is better than that for the two FDOs with $d_2 \leq 160$m and then increases significantly when d_2 is larger. This is because in [25], the stronger source node is always allocated a higher power level, leading to a significant degradation of the weaker source node's performance at higher path-loss. In general, the OOP for our proposed DDO goes up following an increase of d_2 due to the higher path-loss at $\mathcal{S}_2$. Similar to downlink pairwise NOMA, the OOP using our proposed DDO approaches the OOP for the FDO1 with $d_2 \gg d_1$ due to the probability of it being the correct order is approximately one, $p_{RO} \approx 1$. All results in these figures show that the OOP for our proposed DDO scheme performs the best. In addition, we can make the following observations:

- When the distance between the AP and $\mathcal{S}_2$ goes up, the OOP for the FDO1 scheme first decreases and then tends to increase. This is because a greater d_2 leads to a weaker signal from $\mathcal{S}_2$ and also less interference in decoding $\mathcal{S}_1$'s signal. However, when $\mathcal{S}_2$ is too far away

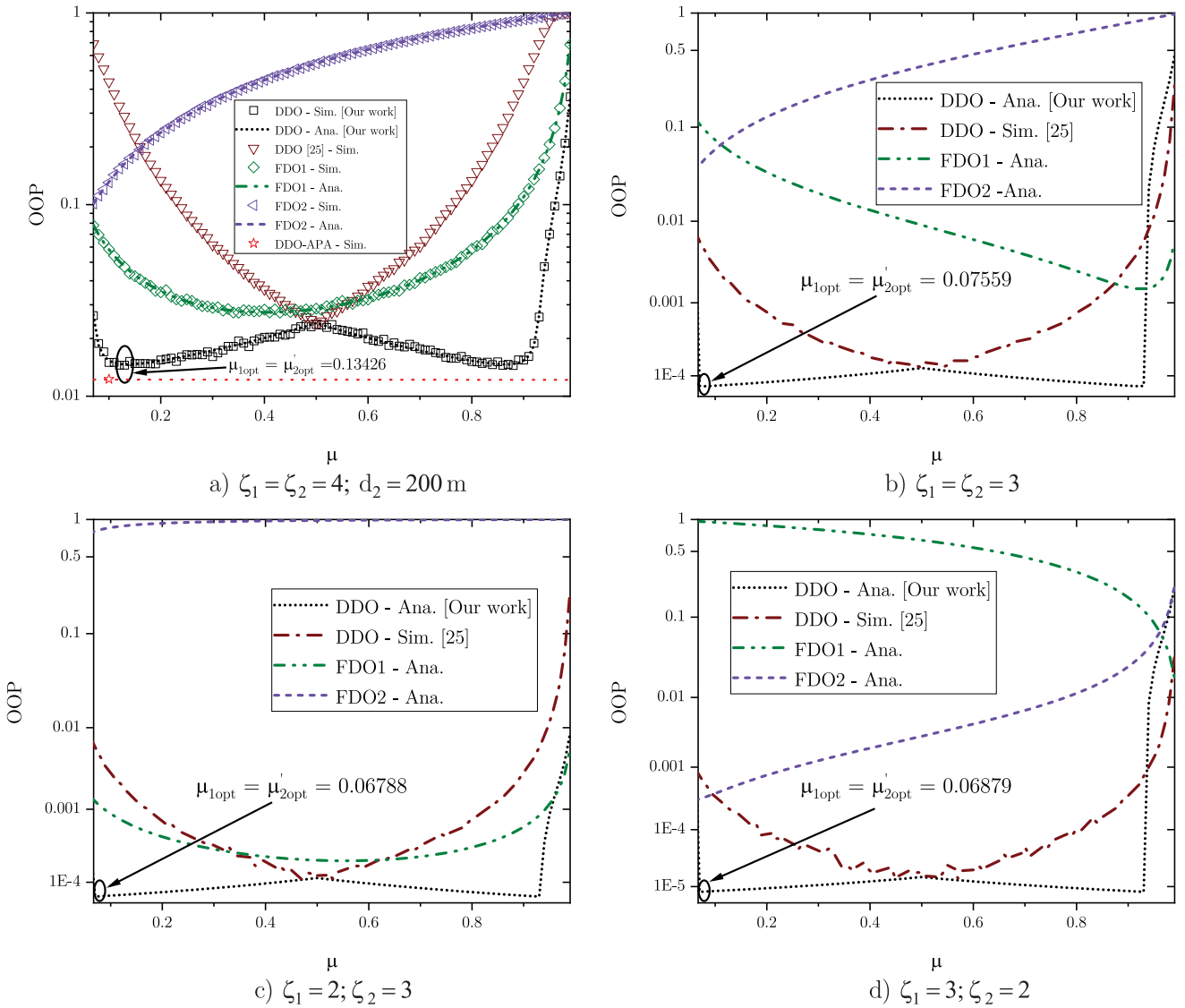

FIGURE 11. The OOP versus μ_1 for the uplink pairwise NOMA, $d_1 = 100$m, $d_2 = 200$m, $R_{1th} = R_{2th} = 0.1$ bps.

from the AP, the probability of unsuccessful decoding $\mathcal{S}_2$'s signal at the AP also goes up. Especially, in Fig. 15d, the OOP for the FDO1 scheme is very high at $d_2 \approx d_1$ due to higher interference from $\mathcal{S}_2$.

- The OOP for the FDO2 experiences a significant increase with growing distance between the AP and $\mathcal{S}_2$ due to the effect of higher path-loss. Moreover, this probability reaches 1 even faster with $\zeta_2 > \zeta_1$, Fig. 15c, due to the reduction of signal-to-interference-plus-noise ratio (SINR). On the other hand, the OOP for FDO2 is better than that for FDO1 at smaller distances between the AP and $\mathcal{S}_2$ with $\zeta_1 = \zeta_2 = 4$, Fig. 15a, as with $\mu'_1 = 0.2$ for FDO2, $\mathcal{S}_2$ is assigned more power than $\mathcal{S}_1$, resulting in an increase of SIC's performance. Meanwhile, for FDO1 when $\mathcal{S}_1$'s signal is decoded first, $\mathcal{S}_1$ is allocated with $\mu_1 = 0.2$ to cope with high path-loss due to $\zeta_1 = 4$. Especially, the OOP for FDO2 is much better than that for FDO1 when $\mathcal{S}_2$ gets more power as well as experiences a better environment, Fig. 15d. We did not see this phenomenon in FDO downlink pairwise NOMA since power allocation plays a very crucial role on the OOP. Thus, with $\mu'_1 < \mu'_2$, the OOP for FDO2 cannot be better than that for FDO1 in downlink pairwise NOMA.
- In different environments, the OOP for the DDO scheme in [25] increases significantly when d_2 increases and performs better compared to both FDOs at $d_2 \approx d_1$. This is because the probability of successfully decoding $\mathcal{S}_2$'s signal with smaller power level is better at the distance $d_2 \approx d_1$. Moreover, when $\mathcal{S}_2$ is located in a better environment compared to $\mathcal{S}_1$, the OOP for the DDO scheme using the power allocation strategy in [25] changes slowly with an increase of d_2, Fig. 15d. The

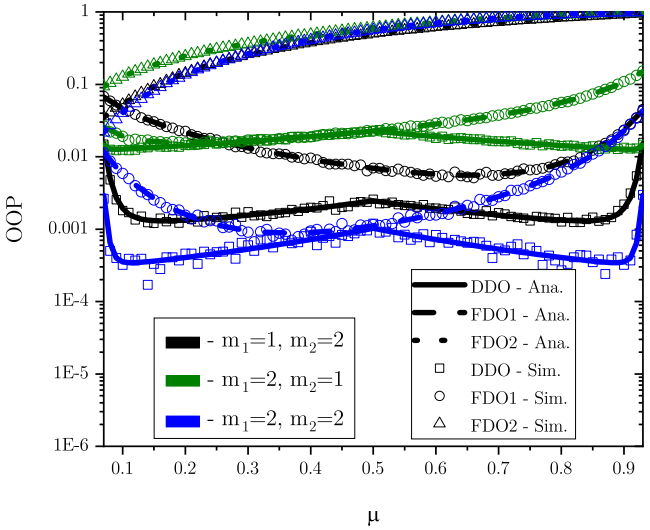

FIGURE 12. The OOP versus μ_1 for the uplink pairwise NOMA, $d_1 = 100$m, $d_2 = 200$m, $\zeta_1 = \zeta_2 = 4$, $R_{1th} = R_{2th} = 0.1$ bps with different shape factors.

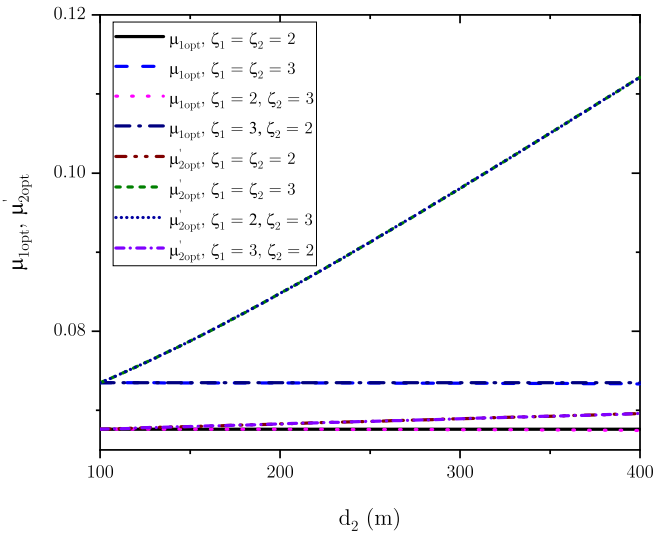

FIGURE 13. The μ_{1opt} and μ'_{2opt} versus d_2 for the uplink pairwise NOMA with $d_1 = 100$m, $\lambda_1 = \lambda_2 = 1$, $R_{1th} = R_{2th} = 0.1$ bps.

reason is that the normalized channel gain between the AP and $\mathcal{S}_2$ becomes much better than $\mathcal{S}_1$.

Similar to downlink pairwise NOMA, the OOP using the DDO-FPPA scheme with $\mu_1 = \mu'_2$ is very close to that using the optimal power allocation strategy $\mu_1 \neq \mu'_2$ as shown in Figs. 15 and 17, while this OOP changes only a little when μ_1 goes up, Fig. 17. Hence, finding the optimal power allocation coefficients for the DDO-FPPA scheme using the power allocation strategy $\mu_1 = \mu'_2$ can help in decreasing the computational load and complexity at the AP.

C. DISCUSSION

The following conclusions can be made from the results presented above:

- The proposed DDO-FPPA scheme is much less complex than the DDO-DPA scheme, while its communication reliability in terms of the OOP is still close to the DDO-DPA scheme.
- In order to reduce the complexity and computational load at the AP, the power allocation strategy with $\mu_1 =$

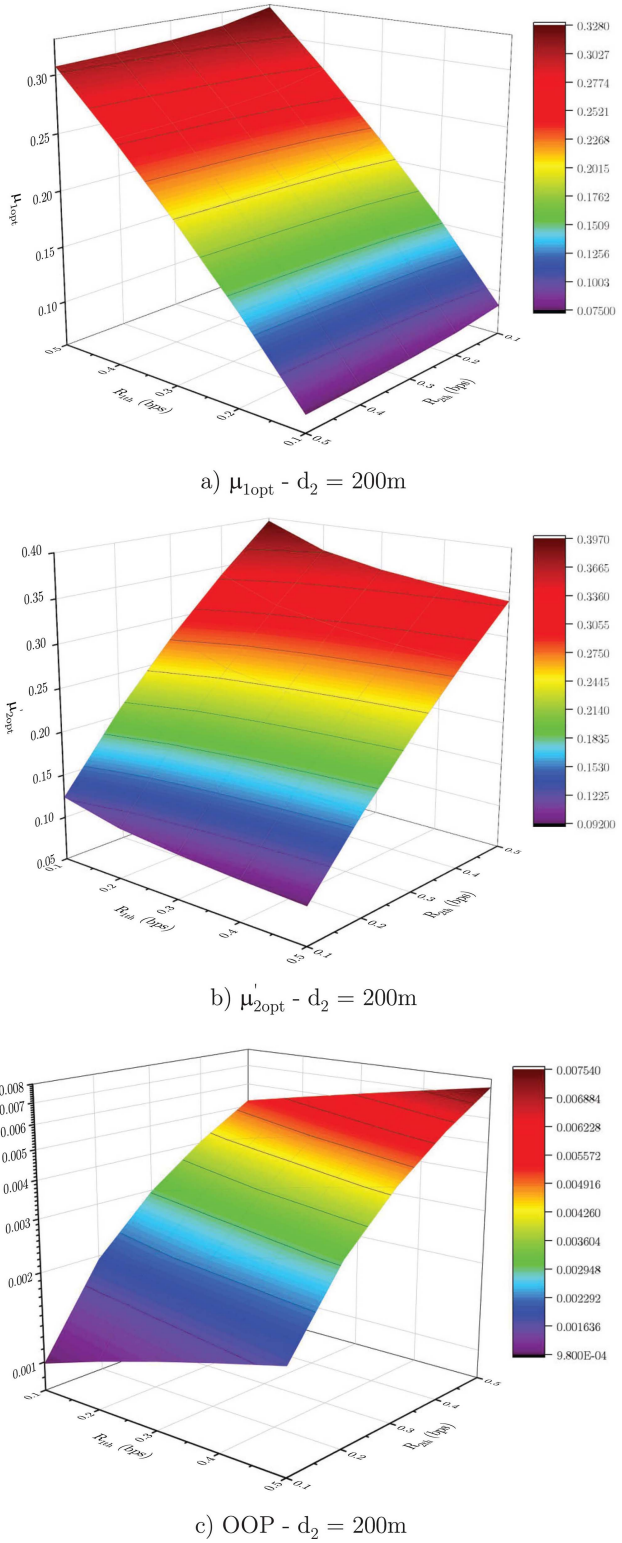

FIGURE 14. The OOP versus R_{1th} for the uplink pairwise NOMA with $d_1 = 100$m, $d_2 = 200$m, $\zeta_1 = \zeta_2 = 3.5$.

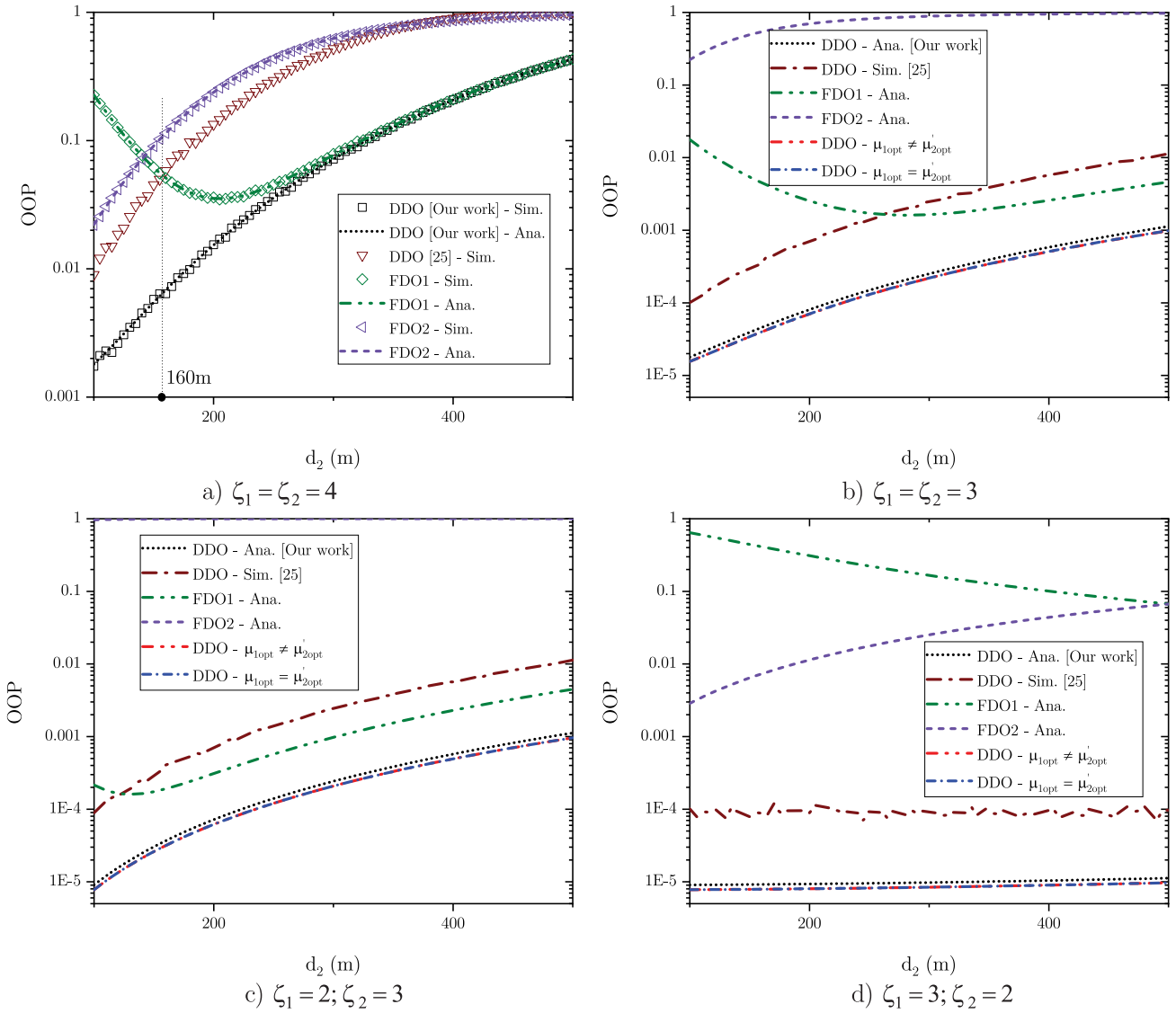

FIGURE 15. The OOP versus d_2 for the uplink pairwise NOMA, $d_1 = 100$m, $\mu_1 = \mu_2' = 0.2$ for the our proposed DDO, $\mu_1 = \mu_1' = 0.2$ for both FDOs, $R_{1th} = R_{2th} = 0.1$ bps.

μ_2' and $\mu_2 = \mu_1'$ should be adopted to find the optimal power allocation factors using **Algorithms 3 and 4**.

- In both uplink and downlink pairwise NOMA, when the proposed DDO schemes are used, the OOP changes slightly with an increase of power allocation factors. In contrast, the OOP for both FDOs changes significantly following a change of power allocation factors.
- To improve the reliability of the communication in terms of OOP, a pair of source nodes should satisfy the condition of $R_{1th} \geq R_{2th}$ when $d_1 \geq d_2$.

VII. CONCLUSION

In this article we consider pairwise NOMA and calculate the OOP for dynamic and fixed decoding orders, for both uplink and downlink scenarios over Nakagami-m fading channels. Further, we propose algorithms to find the optimal fixed power allocation for both nodes in pairwise NOMA using different power allocation strategies. Comparisons in terms of the OOP between the proposed DDO-FPPA schemes and others show that the proposed schemes for both uplink and downlink pairwise NOMA are less complex but still achieve optimal results. The OOPs with and without optimal fixed power allocation are also studied to see how they are affected by the distances between the source nodes and the AP, the target rates and the path-loss exponents. It can be seen that the OOP for the proposed DDO-FPPA scheme is suitable for both uplink and downlink pairwise NOMA due to its optimality and lower complexity.

APPENDIX

A. DERIVATION OF THE PROBABILITY p

In this section, we derive the closed-form expression of the probability p which is defined in Theorem 1. The cumulative distribution function and probability density function of the

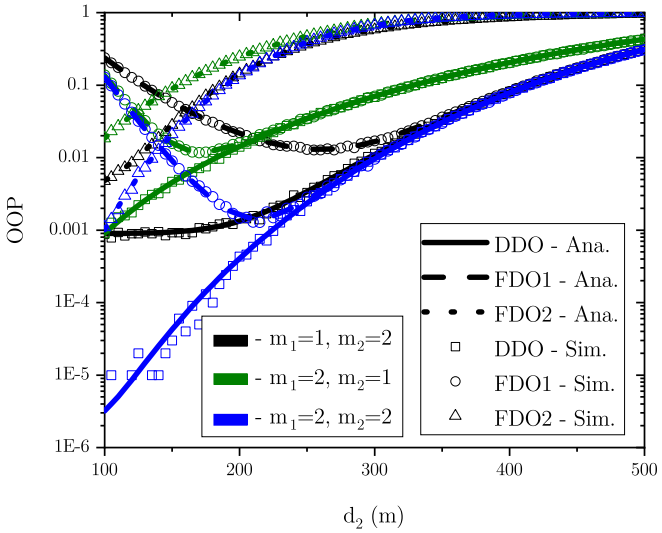

FIGURE 16. The OOP versus d_2 for the uplink pairwise NOMA, $d_1 = 100$m, $\zeta_1 = \zeta_2 = 4$, $\mu_1 = \mu_2' = 0.2$ for the our proposed DDO, $\mu_1 = \mu_1' = 0.2$ for both FDOs, $R_{1th} = R_{2th} = 0.1$ bps with different shape factors.

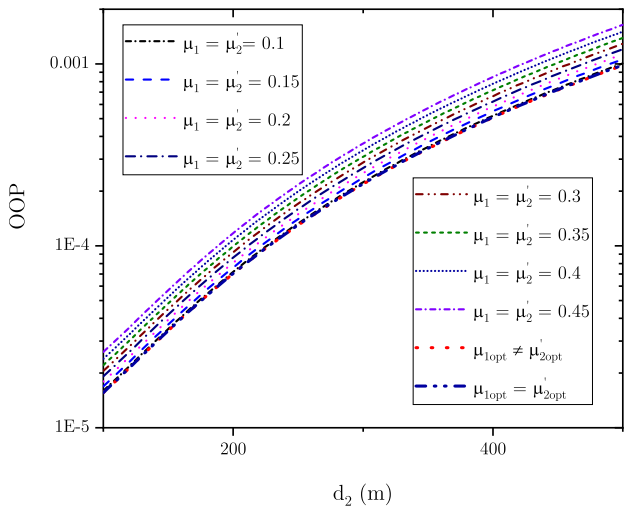

FIGURE 17. The OOP using a DDO versus d_2 for the DDO in uplink pairwise NOMA with $d_1 = 100$m, $\zeta_1 = \zeta_2 = 3$, $R_{1th} = R_{2th} = 0.1$ bps.

random variable $X \sim G(m_X, \frac{\gamma_X}{m_X})$ and $Y \sim G(m_Y, \frac{\gamma_Y}{m_Y})$ are expressed as follows, respectively:

$$F_T(t) = 1 - \frac{\Gamma\left(m_T, m_T\gamma_T^{-1}t\right)}{\Gamma(m_T)}, t > 0, \tag{58}$$

$$f_T(t) = \frac{\left(m_T\gamma_T^{-1}\right)^{m_T} t^{m_T-1}e^{-m_T\gamma_T^{-1}t}}{\Gamma(m_T)}, t > 0, \tag{59}$$

where $T \in \{X, Y\}$ and $t \in \{x, y\}$.

(a) $a \neq 0, b \neq 0, c = 0$:

$$p_a = \Pr\{(X \geq a) \cap (Y \geq bX)\} = \int_a^\infty f_X(x)dx \int_{bx}^\infty f_Y(y)dy$$
$$= \int_a^\infty f_X(x)\frac{\Gamma\left(m_Y, m_Y\gamma_Y^{-1}bx\right)}{\Gamma(m_Y)}dx. \tag{60}$$

Here, the incomplete Gamma function can be represented as $\frac{\Gamma(m_Y, m_Y\gamma_Y^{-1}bx)}{\Gamma(m_Y)} = e^{-m_Y\gamma_Y^{-1}bx}\sum_{i=0}^{m_Y-1}\frac{(m_Y\gamma_Y^{-1}bx)^i}{i!}$ [40, Eq. 8.352.4] given that m_X and m_Y are integers. Substituting into (60), p_a is obtained as in (13) by applying [40, Eq. 3.381.3].

(b) $a = 0, b \neq 0, c = 0$: Similar to calculating p_a, p_b is obtained as in (14).

(c) $a \neq 0, b \neq 0, c \neq 0$:

$$p_c = \Pr\{(X \geq a) \cap (Y \geq bX + c)\}$$
$$= \int_a^\infty f_X(x)dx \int_{bx+c}^\infty f_Y(y)dy$$
$$= \int_a^\infty f_X(x)\frac{\Gamma\left(m_Y, m_Y\gamma_Y^{-1}(bx + c)\right)}{\Gamma(m_Y)}dx, \tag{61}$$

$\frac{\Gamma(m_Y, m_Y\gamma_Y^{-1}(bx+c))}{\Gamma(m_Y)} = e^{-m_Y\gamma_Y^{-1}(bx+c)}\sum_{i=0}^{m_Y-1}\frac{(m_Y\gamma_Y^{-1}(bx+c))^i}{i!}$ [40, Eq. 8.352.4] with m_X and m_Y being integers. Substituting into (61), we have

$$p_c = \frac{\left(m_X\gamma_X^{-1}\right)^{m_X}e^{-m_Y\gamma_Y^{-1}c}}{\Gamma(m_X)}$$
$$\times \sum_{i=0}^{m_Y-1}\frac{\left(m_Y\gamma_Y^{-1}c\right)^i}{i!}\int_a^\infty\left(\frac{b}{c}x + 1\right)^i x^{m_X-1}e^{-\rho x}dx. \tag{62}$$

Applying the binomial theorem, we have $(\frac{b}{c}x + 1)^i = \sum_{j=0}^{i}\binom{i}{j}(\frac{b}{c})^j x^j$ [40, Eq. 1.111]. Thus, p_c is derived as in (15) by applying [40, Eq. 3.381.3].

(d) $a = 0, b \neq 0, c \neq 0$: Similar to case (c), p_d is derived as in (16).

B. THE FIRST DERIVATIVE OF I_{1b}, I_{2b}, I_{3b}, I_{4b} WITH $m_1 = m_2 = 1$

$$\frac{\partial I_{1b}}{\partial\mu_1} = \frac{A_1^d e^{-\frac{A_1^d}{\gamma_1\mu_1}}\left(e^{\frac{A_2^d}{\gamma_2\left(A_2^d\mu_1+\mu_1-1\right)}} - e^{-\frac{A_1 d_2^{\xi_2}}{d_1^{\xi_1}\gamma_1\mu_1}}\right)}{\gamma_1\mu_1^2}$$
$$- e^{-\frac{A_1^d}{\gamma_1\mu_1}}\left(\frac{A_1 d_2^{\xi_2}e^{-\frac{A_1 d_2^{\xi_2}}{d_1^{\xi_1}\gamma_1\mu_1}}}{d_1^{\xi_1}\gamma_1\mu_1^2} + \frac{A_2^d\left(A_2^d+1\right)e^{\frac{A_2^d}{\gamma_2\left(A_2^d\mu_1+\mu_1-1\right)}}}{\gamma_2\left(A_2^d\mu_1+\mu_1-1\right)^2}\right)$$
$$+ \frac{A_1 d_2^{\xi_2}e^{-\frac{A_1^d\left(d_1^{\xi_1}+d_2^{\xi_2}\right)}{d_1^{\xi_1}\gamma_1\mu_1}}}{d_1^{\xi_1}\gamma_1\mu_1^2}. \tag{63}$$

$$\frac{\partial I_{2b}}{\partial\mu_2'} = \left(\frac{A_2^d}{\gamma_2{\mu_2'}^2} - \frac{A_1^d\left(A_1^d+1\right)}{\gamma_1(A_1^d\mu_2' + \mu_2' - 1)^2}\right)$$
$$\times e^{-\frac{A_2^d}{\gamma_2\mu_2'}+\frac{A_1^d}{\gamma_1(A_1^d\mu_2'+\mu_2'-1)}} - \frac{A_2^d e^{-\frac{A_2^d\left(d_1^{\xi_1}+d_2^{\xi_2}\right)}{\gamma_2\mu_2' d_2^{\xi_2}}}}{\gamma_2{\mu_2'}^2}. \tag{64}$$

$$\frac{\partial I_{3b}}{\partial \mu_1} = \frac{\gamma_{t1}\mu_1 e^{\frac{A_2^u}{\gamma_{t2}(\mu_1-1)}-\frac{A_1^u(A_2^u+1)}{\gamma_{t1}\mu_1}}\left[\frac{A_1^u(A_2^u+1)}{\gamma_{t1}{\mu_1}^2}-\frac{A_2^u}{\gamma_{t2}(\mu_1-1)^2}\right]}{\gamma_{t1}\mu_1 - A_1^u\gamma_{t2}(\mu_1-1)} + \frac{\gamma_{t1}e^{\frac{A_2^u}{\gamma_{t2}(\mu_1-1)}-\frac{A_1^u(A_2^u+1)}{\gamma_{t1}\mu_1}}}{\gamma_{t1}\mu_1 - A_1^u\gamma_{t2}(\mu_1-1)}$$
$$- \frac{\gamma_{t1}\mu_1\left(\gamma_{t1}-A_1^u\gamma_{t2}\right)e^{\frac{A_2^u}{\gamma_{t2}(\mu_1-1)}-\frac{A_1^u(A_2^u+1)}{\gamma_{t1}\mu_1}}}{\left[\gamma_{t1}\mu_1 - A_1^u\gamma_{t2}(\mu_1-1)\right]^2} + \left(\frac{\gamma_{t1}\mu_1\left(\gamma_{t1}-A_1^u\gamma_{t2}\right)}{\left[\gamma_{t1}\mu_1 - A_1^u\gamma_{t2}(\mu_1-1)\right]^2} - \frac{\gamma_{t1}}{\gamma_{t1}\mu_1 - A_1^u\gamma_{t2}(\mu_1-1)}\right)$$
$$\times e^{-\frac{A_1^u\left(d_1^{\zeta_1}+d_2^{\zeta_2}\right)d_2^{-\zeta_2}}{A_1^u\gamma_{t2}(\mu_1-1)+b_2\gamma_{t1}\mu_1}} + \frac{A_1^u\left(d_1^{\zeta_1}+d_2^{\zeta_2}\right)\left(A_1^u\gamma_{t2}d_2^{\zeta_2}+d_1^{\zeta_1}\gamma_{t1}\right)e^{-\frac{A_1^u\left(d_1^{\zeta_1}+d_2^{\zeta_2}\right)}{A_1^u\gamma_{t2}d_2^{\zeta_2}(\mu_1-1)+d_1^{\zeta_1}\gamma_{t1}\mu_1}}\left(\frac{d_2^{\zeta_2}}{d_1^{\zeta_1}+d_2^{\zeta_2}}-\frac{\gamma_{t1}\mu_1}{\gamma_{t1}\mu_1-A_1^u\gamma_{t2}(\mu_1-1)}\right)}{\left[A_1^u\gamma_{t2}(\mu_1-1)d_2^{\zeta_2}+d_1^{\zeta_1}\gamma_{t1}\mu_1\right]^2} \tag{65}$$

$$\frac{\partial I_{4b}}{\partial \mu_2'} = \frac{\gamma_{t2}e^{-\frac{A_2^u}{\gamma_{t2}\mu_2'}}\left(e^{A_1^u\left(\frac{1}{\gamma_{t1}\left(\mu_2'-1\right)}-\frac{A_2^u}{\gamma_{t2}\mu_2'}\right)} - e^{\frac{A_2^u d_1^{\zeta_1}\left[A_2^u\gamma_{t1}\left(\mu_2'-1\right)-\gamma_{t2}\mu_2'\right]}{\gamma_{t2}\mu_2'\left[A_2^u d_1^{\zeta_1}\gamma_{t1}\left(\mu_2'-1\right)+\gamma_{t2}\mu_2' d_2^{\zeta_2}\right]}}\right)}{\gamma_{t2}\mu_2' - A_2^u\gamma_{t1}\left(\mu_2'-1\right)}$$
$$+ \frac{\gamma_{t2}\mu_2' e^{-\frac{A_2^u}{\gamma_{t2}\mu_2'}}\left[-\left(\begin{array}{c} -\frac{A_2^u d_1^{\zeta_1}\left[A_2^u\gamma_{t1}\left(\mu_2'-1\right)-\gamma_{t2}\mu_2'\right]}{\gamma_{t2}{\mu_2'}^2\left[A_2^u d_1^{\zeta_1}\gamma_{t1}\left(\mu_2'-1\right)+d_2^{\zeta_2}\gamma_{t2}\mu_2'\right]} + \frac{A_2^u d_1^{\zeta_1}\left(A_2^u\gamma_{t1}-\gamma_{t2}\right)}{\gamma_{t2}\mu_2'\left[A_2^u d_1^{\zeta_1}\gamma_{t1}\left(\mu_2'-1\right)+d_2^{\zeta_2}\gamma_{t2}\mu_2'\right]} \\ -\frac{A_2^u d_1^{\zeta_1}\left(A_2^u d_1^{\zeta_1}\gamma_{t1}+d_2^{\zeta_2}\gamma_{t2}\right)\left[A_2^u\gamma_{t1}\left(\mu_2'-1\right)-\gamma_{t2}\mu_2'\right]}{\gamma_{t2}\mu_2'\left[A_2^u d_1^{\zeta_1}\gamma_{t1}\left(\mu_2'-1\right)+d_2^{\zeta_2}\gamma_{t2}\mu_2'\right]^2} \end{array}\right)e^{\frac{A_2^u d_1^{\zeta_1}\left[A_2^u\gamma_{t1}\left(\mu_2'-1\right)-\gamma_{t2}\mu_2'\right]}{\gamma_{t2}\mu_2'\left[A_2^u d_1^{\zeta_1}\gamma_{t1}\left(\mu_2'-1\right)+d_2^{\zeta_2}\gamma_{t2}\mu_2'\right]}}\right]}{\gamma_{t2}\mu_2' - A_2^u\gamma_{t1}\left(\mu_2'-1\right)}$$
$$+ \frac{A_2^u e^{-\frac{A_2^u}{\gamma_{t2}\mu_2'}}\left[e^{A_1^u\left(\frac{1}{\gamma_{t1}\left(\mu_2'-1\right)}-\frac{A_2^u}{\gamma_{t2}\mu_2'}\right)} - e^{\frac{A_2^u d_1^{\zeta_1}\left[A_2^u\gamma_{t1}\left(\mu_2'-1\right)-\gamma_{t2}\mu_2'\right]}{\gamma_{t2}\mu_2'\left[A_2^u d_1^{\zeta_1}\gamma_{t1}\left(\mu_2'-1\right)+d_2^{\zeta_2}\gamma_{t2}\mu_2'\right]}}\right]}{\mu_2'\left[\gamma_{t2}\mu_2' - A_2^u\gamma_{t1}\left(\mu_2'-1\right)\right]} + \frac{A_2^u d_1^{\zeta_1}\left(A_2^u d_1^{\zeta_1}\gamma_{t1}+d_2^{\zeta_2}\gamma_{t2}\right)e^{-\frac{A_2^u\left(d_1^{\zeta_1}+d_2^{\zeta_2}\right)}{A_2^u d_1^{\zeta_1}\gamma_{t1}\left(\mu_2'-1\right)+d_2^{\zeta_2}\gamma_{t2}\mu_2'}}}{\left[A_2^u d_1^{\zeta_1}\gamma_{t1}\left(\mu_2'-1\right)+d_2^{\zeta_2}\gamma_{t2}\mu_2'\right]^2}$$
$$- \frac{\gamma_{t2}\mu_2' e^{-\frac{A_2^u}{\gamma_{t2}\mu_2'}}\left(\gamma_{t2}-A_2^u\gamma_{t1}\right)\left[e^{A_1^u\left(\frac{1}{\gamma_{t1}\left(\mu_2'-1\right)}-\frac{A_2^u}{\gamma_{t2}\mu_2'}\right)} - e^{\frac{A_2^u d_1^{\zeta_1}\left[A_2^u\gamma_{t1}\left(\mu_2'-1\right)-\gamma_{t2}\mu_2'\right]}{\gamma_{t2}\mu_2'\left[A_2^u d_1^{\zeta_1}\gamma_{t1}\left(\mu_2'-1\right)+d_2^{\zeta_2}\gamma_{t2}\mu_2'\right]}}\right]}{\left[\gamma_{t2}\mu_2' - A_2^u\gamma_{t1}\left(\mu_2'-1\right)\right]^2} \tag{66}$$

REFERENCES

[1] Y. Yuan, Y. Zhao, B. Zong, and S. Parolari, "Potential key technologies for 6G mobile communications," *Sci. China Inf. Sci.*, vol. 63, pp. 1–19, May 2020.

[2] C. Huang *et al.*, "Holographic MIMO surfaces for 6G wireless networks: Opportunities, challenges, and trends," *IEEE Wireless Commun.*, vol. 27, no. 5, pp. 118–125, Oct. 2020.

[3] C. Huang, A. Zappone, G. C. Alexandropoulos, M. Debbah, and C. Yuen, "Reconfigurable intelligent surfaces for energy efficiency in wireless communication," *IEEE Trans. Wireless Commun.*, vol. 18, no. 8, pp. 4157–4170, Aug. 2019.

[4] K. Senel, H. V. Cheng, E. Björnson, and E. G. Larsson, "What role can NOMA play in massive MIMO?" *IEEE J. Sel. Topics Signal Process.*, vol. 13, no. 3, pp. 597–611, Jun. 2019.

[5] T. Hou, Y. Liu, Z. Song, X. Sun, and Y. Chen, "MIMO-NOMA networks relying on reconfigurable intelligent surface: A signal cancellation based design," *IEEE Trans. Commun.*, vol. 68, no. 11, pp. 6932–6944, Nov. 2020, doi: 10.1109/tcomm.2020.3018179.

[6] M. Bennis, M. Debbah, and H. V. Poor, "Ultrareliable and low-latency wireless communication: Tail, risk, and scale," *Proc. IEEE*, vol. 106, no. 10, pp. 1834–1853, Oct. 2018.

[7] G. Song and X. Wang, "Comparison of interference cancellation schemes for non-orthogonal multiple access system," in *Proc. IEEE Veh. Technol. Conf.*, Nanjing, China, May 2016, pp. 1–5.

[8] L. Dai, B. Wang, Y. Yuan, S. Han, I. Chih-Lin, and Z. Wang, "Non-orthogonal multiple access for 5G: solutions, challenges, opportunities, and future research trends," *IEEE Commun. Mag.*, vol. 53, no. 9, pp. 74–81, Sep. 2015.

[9] L. Y. Hosni, A. Y. Farid, A. A. Elsaadany, and M. A. Safwat, "5G new radio prototype implementation based on SDR," *Commun. Netw.*, vol. 12, no. 1, pp. 1–27, 2019.

[10] A. Benjebbour, A. Li, K. Saito, Y. Saito, Y. Kishiyama, and T. Nakamura, "NOMA: From concept to standardization," in *Proc. Conf. Stand. Commun. Netw.*, Tokyo, Japan, Oct. 2015, pp. 18–23.

[11] X. Wei *et al.*, "Software defined radio implementation of a non-orthogonal multiple access system towards 5G," *IEEE Access*, vol. 4, pp. 9604–9613, 2016.

[12] X. Xiong, W. Xiang, K. Zheng, H. Shen, and X. Wei, "An open source SDR-based NOMA system for 5G networks," *IEEE Wireless Commun.*, vol. 22, no. 6, pp. 24–32, Dec. 2015.

[13] H. Pan, L. Lu, and S. C. Liew, "Practical power-balanced non-orthogonal multiple access," *IEEE J. Sel. Areas Commun.*, vol. 35, no. 10, pp. 2312–2327, Oct. 2017.

[14] S. Abeywickrama, L. Liu, Y. Chi, and C. Yuen, "Over-the-air implementation of uplink NOMA," in *Proc. IEEE Global Commun. Conf.*, Singapore, Dec. 2017, pp. 1–6.
[15] Z. Ding, P. Fan, and H. V. Poor, "Impact of user pairing on 5G nonorthogonal multiple-access downlink transmissions," *IEEE Trans. Veh. Technol.*, vol. 65, no. 8, pp. 6010–6023, Aug. 2016.
[16] L. Zhu, J. Zhang, Z. Xiao, X. Cao, and D. O. Wu, "Optimal user pairing for downlink non-orthogonal multiple access (NOMA)," *IEEE Wireless Commun. Lett.*, vol. 8, no. 2, pp. 328–331, Apr. 2019.
[17] Z. Ding, R. Schober, and H. V. Poor, "A general MIMO framework for NOMA downlink and uplink transmission based on signal alignment," *IEEE Trans. Wireless Commun.*, vol. 15, no. 6, pp. 4438–4454, Jun. 2016.
[18] X. Chen, G. Liu, Z. Ma, X. Zhang, W. Xu, and P. Fan, "Optimal power allocations for non-orthogonal multiple access over 5G full/half-duplex relaying mobile wireless networks," *IEEE Trans. Wireless Commun.*, vol. 18, no. 1, pp. 77–92, Jan. 2019.
[19] F. Liu and M. Petrova, "Dynamic power allocation for downlink multi-carrier NOMA systems," *IEEE Commun. Lett.*, vol. 22, no. 9, pp. 1930–1933, Sep. 2018.
[20] A. Benjebbour, K. Saito, A. Li, Y. Kishiyama, and T. Nakamura, "Non-orthogonal multiple access (NOMA): Concept and design," in *Proc. Signal Process. 5G Algorithms Implement.*, Chichester, U.K., 2016, pp. 143–168.
[21] P. Xu, Y. Yuan, Z. Ding, X. Dai, and R. Schober, "On the outage performance of non-orthogonal multiple access with 1-bit feedback," *IEEE Trans. Wireless Commun.*, vol. 15, no. 10, pp. 6716–6730, Oct. 2016.
[22] G. Li, D. Mishra, and H. Jiang, "Cooperative NOMA with incremental relaying: Performance analysis and optimization," *IEEE Trans. Veh. Technol.*, vol. 67, no. 11, pp. 11291–11295, Nov. 2018.
[23] G. Li and D. Mishra, "Cooperative NOMA networks: User cooperation or relay cooperation?" in *Proc. IEEE Int. Conf. Commun.*, Dublin, Ireland, 2020, pp. 1–6.
[24] P. Xu, Z. Yang, Z. Ding, and Z. Zhang, "Optimal relay selection schemes for cooperative NOMA," *IEEE Trans. Veh. Technol.*, vol. 67, no. 8, pp. 7851–7855, Aug. 2018.
[25] Y. Gao, B. Xia, K. Xiao, Z. Chen, X. Li, and S. Zhang, "Theoretical analysis of the dynamic decode ordering sic receiver for uplink NOMA systems," *IEEE Commun. Lett.*, vol. 21, no. 10, pp. 2246–2249, Oct. 2017.
[26] J. Wang, B. Xia, K. Xiao, Y. Gao, and S. Ma, "Outage performance analysis for wireless non-orthogonal multiple access systems," *IEEE Access*, vol. 6, pp. 3611–3618, 2018.
[27] D. Do, T. Nguyen, S. Ekin, Z. Kaleem, and M. Voznak, "Joint user grouping and decoding order in uplink/downlink MISO/SIMO-NOMA," *IEEE Access*, vol. 8, pp. 143632–143643, 2020.
[28] Z. Ding, H. Dai, and H. V. Poor, "Relay selection for cooperative NOMA," *IEEE Wireless Commun. Lett.*, vol. 5, no. 4, pp. 416–419, Aug. 2016.
[29] Z. Yang, Z. Ding, Y. Wu, and P. Fan, "Novel relay selection strategies for cooperative NOMA," *IEEE Trans. Veh. Technol.*, vol. 66, no. 11, pp. 10114–10123, Nov. 2017.
[30] Z. Yang, Z. Ding, P. Fan, and N. Al-Dhahir, "A general power allocation scheme to guarantee quality of service in downlink and uplink NOMA systems," *IEEE Trans. Wireless Commun.*, vol. 15, no. 11, pp. 7244–7257, Nov. 2016.
[31] Z. Ding, M. Peng, and H. V. Poor, "Cooperative non-orthogonal multiple access in 5G systems," *IEEE Commun. Lett.*, vol. 19, no. 8, pp. 1462–1465, Aug. 2015.
[32] K. Senel and S. Tekinay, "Optimal power allocation in NOMA systems with imperfect channel estimation," in *Proc. IEEE Global Commun. Conf.*, Singapore, Dec. 2017, pp. 1–7.
[33] M. M. El-Sayed, A. S. Ibrahim, and M. M. Khairy, "Power allocation strategies for non-orthogonal multiple access," in *Proc. Int. Conf. Sel. Topics Mobile Wireless Netw.*, Cairo, Egypt, Apr. 2016, pp. 1–6.
[34] C. Aliprantis and K. Border, *Infinite Dimensional Analysis: A Hitchhiker's Guide*. Heidelberg, Germany: Springer, 2013.
[35] J. C. Ehiwario, "Comparative study of bisection, Newton–Raphson and secant methods of root-finding problems," *IOSR J. Eng.*, vol. 4, no. 4, pp. 1–7, 2014.
[36] *Wolfram Mathematica*. Accessed: Aug. 31, 2020. [Online]. Available: https://www.wolfram.com/mathematica/
[37] A. Dey, "Mathematical model formulation and comparison study of various methods of root-finding problems," *IOSR J. Math.*, vol. 11, no. 2, pp. 64–71, 2015.
[38] I. Azure, G. Aloliga, and L. Doabil, "Comparative study of numerical methods for solving non-linear equations using manual computation," *Math. Lett.*, vol. 5, no. 4, pp. 41–46, 2019.
[39] H. Tabassum, M. S. Ali, E. Hossain, M. J. Hossain, and D. I. Kim, "Uplink vs. downlink NOMA in cellular networks: Challenges and research directions," in *Proc. IEEE Veh. Technol. Conf.*, Sydney, NSW, Australia, 2017, pp. 1–7.
[40] I. S. Gradshteyn and I. M. Ryzhik, *Table of Integrals, Series, and Products*, 7th ed. Amsterdam, The Netherlands: Elsevier, 2007.

VAN-LAN DAO (Graduate Student Member, IEEE) received the B.S. degree in electrical and electronic engineering from Le Quy Don Technical University, Ha Noi, Vietnam, in 2011, and the M.S. degree in automation and control engineering from Le Quy Don Technical University, Ha Noi, Vietnam, in 2016. He is currently pursuing the Ph.D. degree with the Data Communications Group, School of Innovation, Design and Engineering, Malardalen University, Västeräs, Sweden. His research interests include embedded system design for Internet of Things (IoT), wireless sensor networks (WSN), wireless body area networks (WBAN), hardware security, digital VLSI/ASIC design and FPGA-based system hardware design, non-orthogonal multiple access, and timely and reliable communication for wireless networks.

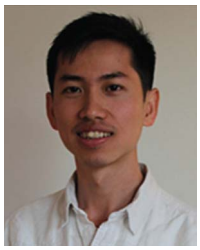

LE-NAM HOANG (Member, IEEE) received the B.Eng. degree in electronics and telecommunications from the Hanoi University of Technology, Vietnam, in 2007, the M.Sc. degree in electrical engineering from the Blekinge Institute of Technology, Sweden, in 2010, and the Ph.D. degree in computer science and engineering from Halmstad University, Sweden, in 2017. He is currently a Postdoctoral Fellow with the School of Innovation, Design and Engineering, Malardalen University, Västeräs, Sweden. His research interests include non-orthogonal multiple access and relaying strategies, under the constraints of timeliness, reliability, and security for wireless communications in safety-critical applications.

SVETLANA GIRS (Member, IEEE) received the B.Sc. and M.Sc. degrees in telecommunications from Saint-Petersburg State Polytechnic University, Russia, in 2009 and 2011, respectively, and the Ph.D. degree in computer science and engineering from Malardalen University in 2016. She is a Lecturer with the School of Innovation, Design and Engineering, Malardalen University, Västeräs, Sweden, where she is currently leading the Networked and Embedded Systems Division. She has been a Visiting Researcher with the University of Canterbury, Christchurch, New Zealand for three months in 2014. Her research interests include real-time communication, cooperative relay networks and reliable wireless communication for industrial systems. She is also a Co-Chair of the Subcommittee on Industrial Communication Systems within the IEEE IES Technical Committee on Factory Automation.

ELISABETH UHLEMANN (Senior Member, IEEE) received the Ph.D. degree in communications theory from the Chalmers University of Technology, Gothenburg, Sweden, in 2004. She has held Visiting positions with the University of South Australia in 2005, the Technical University of Berlin in 2007, and the University of Canterbury, New Zealand, in 2011. She has also worked as a Consultant with Volvo Technology from 2005 to 2009, dealing with connected vehicles, as a Consultant with Ikanos Communications, CA, USA, in 2005, with VDSL protocols and with Free2move, Sweden, from 2009 to 2010, and with wireless audio. She is currently a Full Professor in Data Communications with Malardalen University, Sweden. She has been involved in several European Projects studying communication requirements for traffic-safety applications in vehicular networks. She also contributed to the European ITS communications architecture and has served as a Technical Expert in Standardization within ETSI TC ITS. She currently serves as a Senior Editor for *IEEE TVT Magazine* on Connected and Automated Vehicles and has served as a Member of different Ph.D. examination committees over 20 times in five different countries. She is the Vice Chair of the Swedish VT/COM/IT Chapter.